Indo-Pacific Ocean response to atmospheric intraseasonal variability: 1. Austral summer and the Madden-Julian Oscillation

Duane E. Waliser
Marine Sciences Research Center, State University of New York, Stony Brook, New York, USA

Ragu Murtugudde
Earth System Science Interdisciplinary Center, University of Maryland, College Park, Maryland, USA

Lisanne E. Lucas
Marine Sciences Research Center, State University of New York, Stony Brook, New York, USA

Received 30 August 2002; revised 19 December 2002; accepted 4 February 2003; published 24 May 2003.

[1] The large-scale response of the Indo-Pacific Ocean to atmospheric forcing associated with the Madden-Julian Oscillation (MJO) is examined using an ocean general circulation model forced by canonical MJO conditions constructed from observations. The results show that for a number of equatorial areas, ocean advection processes can play an important role in determining the ocean response. In addition, mixed layer depth (MLD) variations are considerable and contribute to the sea surface temperature (SST) variability. SST variability also develops in the eastern equatorial Pacific via the propagation of ocean Kelvin waves. With regards to this variability the results suggest that advective processes, namely, meridional advection, play the most significant role. Sea level variability in the equatorial regions and eastern sides of the Indian and Pacific basins associated with the MJO is considerable. In conjunction with these sea level variations are also large variations in the Indonesian Throughflow. The results also show that the MJO forcing produces a low-frequency rectified signal consisting of a weak cooling in the equatorial western Pacific and Indian Ocean regions, a relatively larger warming around the maritime continent, a fair amount of MLD shallowing in most of the above regions, and a westward equatorial Pacific Ocean current anomaly. In addition, the heat flux variations associated with the MJO produce systematic variations in the east-west zonal gradient of Indian Ocean SST, which could influence the evolution of the Indian Ocean Zonal Mode. The implications and caveats associated with these results, the caveats associated with the model and forcing framework, and areas necessitating further study are discussed. *INDEX TERMS:* 1620 Global Change: Climate dynamics (3309); 3337 Meteorology and Atmospheric Dynamics: Numerical modeling and data assimilation; 4255 Oceanography: General: Numerical modeling; 4504 Oceanography: Physical: Air/sea interactions (0312); 4572 Oceanography: Physical: Upper ocean processes; *KEYWORDS:* Madden-Julian Oscillation, rectification, tropical oceanography, equatorial currents, ocean-atmosphere interaction

Citation: Waliser, D. E., R. Murtugudde, and L. E. Lucas, Indo-Pacific Ocean response to atmospheric intraseasonal variability: 1. Austral summer and the Madden-Julian Oscillation, *J. Geophys. Res.*, *108*(C5), 3160, doi:10.1029/2002JC001620, 2003.

1. Introduction

[2] During austral summer, the dominant form of intraseasonal variability occurring in the Tropical atmosphere is associated with the Madden-Julian Oscillation (MJOs) [e.g., *Hendon and Salby*, 1994; *Madden and Julian*, 1994]. In recent years, the interaction of the MJO and the ocean has become an increasingly important consideration with regards to our understanding of both weather and climate and our ability to simulate them. This is due to the MJO's extensive interactions with other components of our weather/climate system, in conjunction with evidence that the ocean plays an important role in defining the characteristics of the MJO. In regards to the former, the onset and break activity of the Asian-Australian monsoon system is strongly influenced by the propagation and evolution of MJO events [e.g., *Yasunari*, 1980; *Lau and Chan*, 1986b; *Hendon and Liebmann*, 1990a, 1990b]. The development of persistent North Pacific circulation anomalies during boreal winter, and their influence on extreme precipitation events along the western United States, has been linked to the evolution and eastward progression of convective anomalies associated with the MJO [e.g., *Weickmann*, 1983; *Liebmann and Hartmann*, 1984; *Weickmann et al.*, 1985; *Lau and Phillips*, 1986; *Higgins and Schubert*, 1996; *Higgins and Mo*, 1997; *Mo and Higgins*, 1998b, 1998c; *Higgins et al.*, 2000; *Jones*, 2000]. Similarly, MJO convective activity has

0148-0227/03/2002JC001620$09.00

been linked to Northern Hemisphere summertime precipitation variability over Mexico and South America as well as to austral wintertime circulation anomalies over the Pacific - South American Sector [e.g., *NoguesPaegle and Mo*, 1997; *Mo and Higgins*, 1998a; *Jones and Schemm*, 2000; *Mo*, 2000; *Paegle et al.*, 2000]. Studies have also shown that particular phases of the MJO are more favorable to the development of tropical storms/hurricanes in both the Atlantic and Pacific sectors [*Maloney and Hartmann*, 2000a, 2000b; *Higgins and Shi*, 2001]. Finally, the passage of MJO events over the western Pacific Ocean has been found to significantly modify the thermocline structure in the equatorial eastern Pacific Ocean via their connection to westerly wind bursts [e.g., *McPhaden et al.*, 1988; *McPhaden and Taft*, 1988; *Kessler et al.*, 1995; *Hendon et al.*, 1998]. This latter interaction has even been suggested to play an important role in triggering variations in El Nino-Southern Oscillation (ENSO) [e.g., *Lau and Chan*, 1986a; *Weickmann*, 1991; *Kessler et al.*, 1995; *McPhaden*, 1999; *Kessler and Kleeman*, 2000].

[3] From the discussion above, it is evident that the MJO is an intrinsic mode of variability whose influence is significant and widespread, and involves timescales well outside the intraseasonal band. Unfortunately, there are still significant shortcomings in regards to the ability of atmospheric general circulation models (GCMs) to properly represent the MJO [e.g., *Slingo et al.*, 1996; *Waliser et al.*, 2003]. Yet, there is growing evidence that intraseasonal SST variability seemingly forced by MJO events [e.g., *Krishnamurti et al.*, 1988; *Waliser*, 1996; *Weller and Anderson*, 1996; *Zhang*, 1996; *Hendon and Glick*, 1997; *Lau and Sui*, 1997; *Jones et al.*, 1998; *Shinoda et al.*, 1998; *Woolnough et al.*, 2000] may in turn provide an important feedback to these systems. For example, the numerical study of *Flatau et al.* [1997] employed a simplified atmospheric GCM [*Lau and Peng*, 1987] coupled to an empirically derived slab ocean mixed layer feedback. They found that the addition of the SST feedback produced a significantly stronger and more organized form of intraseasonal variability. Similarly, *Waliser et al.* [1999] compared the MJO characteristics between an atmospheric GCM (AGCM) simulation using specified climatological SSTs and a simulation coupled to a weakly interacting slab ocean mixed layer. Their results showed that the simplified interactive SST produced a better MJO simulation with respect to a number of shortcomings that typify most AGCM simulations of the MJO. These improvements included: 1) stronger intraseasonal variability associated with the MJO, 2) a tendency for the timescales of the modeled MJO to more closely match and consolidate around the observed timescales, 3) a reduced eastward phase speed in the warm pool regions, and 4) an increased seasonal signature in the MJO with relatively more events occurring in the December–May period. While there is some similarity between the implications of Flatau et al. and Waliser et al., each greatly simplified the oceanic processes. A slightly more complete treatment of the ocean was included in the theoretical study of *Wang and Xie* [1998]. In that study, idealized models of the atmosphere and ocean mixed layer (i.e., Kraus-Turner) were coupled. The result was that the SST feedback from wind-driven entrainment/evaporation, and to a lesser extent from the clouds/radiation, was found to be responsible for slowing and destabilizing what would otherwise be a neutral moist atmospheric Kelvin wave in the uncoupled model.

[4] Related to the above SST coupling issue are the findings from two more recent studies. In the first, *Hendon* [2000] coupled a one-dimensional mixed layer model to each ocean grid point of the R30 GFDL climate model [cf. *Hayashi and Golder*, 1997] and found that the coupled mixed layer had virtually no impact on the modeled MJO. However, analysis of the model results showed that the simulated MJO-induced latent heat flux anomalies were relatively incoherent and did not exhibit the proper (i.e., observed) phase relationship relative to the convection, in part because of the model's basic state. Thus the latent heat flux anomalies did not constructively interact with the MJO-induced shortwave anomalies to produce the needed/observed systematic changes in the anomalous SST which in turn could influence the MJO. Thus rather than have implications on the SST-MJO coupling questions, this study's findings helped highlight the necessity for a proper representation of the basic state when simulating the MJO. In the second study, *Kemball-Cook et al.* [2002] coupled a 2.5 layer ocean model to the ECHAM4 AGCM to examine the SST coupling issue for the northeastward propagating mode of intraseasonal variability that is common during boreal summer [*Wang and Rui*, 1990; *Wang and Xie*, 1997]. While this mode of variability is of a somewhat different dynamical nature, they found that coupled SSTs were critical for producing realistic propagation characteristics. For the most part, each of the studies described above points to the important role that intraseasonal SST variations have on the simulation/character of the MJO; however, they all tend to simplify the oceanic processes involved.

[5] The discussion above highlights the need for a robust understanding of the ocean's role in the development and maintenance of the atmospheric intraseasonal variability, namely the MJO. In particular, given the variety of (simplified) methods used to represent the ocean under coupled scenarios it is crucial to have a rather complete assessment of the oceanic response to the sort of intraseasonal forcing associated with the MJO; this includes both ocean dynamics and complete mixed layer physics. To date a number of studies have addressed various aspects of this question. For example, *Shinoda and Hendon* [1998] examined the degree to which a simple mixed layer model could capture the SST variability associated with MJO-related surface flux forcing. To first order, they found that over the bulk of the western Pacific, and to some extent the Indian Ocean, there was fairly good agreement between the model predicted and observed SSTs. *Shinoda and Hendon* [2001] went on to estimate the complete surface heat budget in a localized area of the western Pacific Ocean budget using a Pacific-only ocean GCM (OGCM). They concluded that on the scale of the atmospheric MJO, at least for this area of the Pacific, surface temperature variations are primarily controlled by vertical processes and surface heat flux variations. This latter study was in response to a number of studies [e.g., *Cronin and McPhaden*, 1997; *Ralph et al.*, 1997; *Feng et al.*, 2000] that concluded that horizontal advection processes can make important contributions to the heat and salt budgets of the surface ocean in the western Pacific Ocean under MJO forcing conditions. A number of additional studies have examined the detailed dynamic response

of the near-equatorial Pacific Ocean to various types of intraseasonal wind forcing, often in the context of Kelvin wave activity and the development of El Nino [*Eriksen et al.*, 1983; *Giese and Harrison*, 1991; *Eriksen*, 1993; *Kindle and Phoebus*, 1995; *Zhang and Rothstein*, 1998].

[6] Notwithstanding the above studies, there are still a number of outstanding questions that need to be addressed and/or need continued treatment given model sensitivities and uncertainties associated with observations of atmospheric forcing and ocean response. For example, few, if any, studies have clearly illustrated the totality of ocean variability that might be expected from MJO forcing. This includes determining what aspects of the atmospheric forcing (e.g., rainfall, cloud, evaporation, and wind) and oceanic response (e.g., mixed layer entrainment and vertical/horizontal advection) are the most critical for simulating the observed intraseasonal response in SST and how this depends on ocean basin and region? Considering this question in conjunction with the coupled SST MJO studies discussed above, it would be useful to know for example how well slab ocean physics capture the ocean response to the MJO. In addition, few studies have addressed the manner the MJO might influence basin-wide transport quantities (e.g., Indonesian Throughflow). Moreover, only a few have addressed the rectification of the MJO on the interannual timescale and only one has examined how the MJO might influence the mean state of the ocean [*Kessler and Kleeman*, 2000]. In this regard, does the ocean carry a subsurface memory from one MJO event to the next, or from a set of events from one year to the next? This question regarding rectification to longer timescales may be important when considering recent studies by *Slingo et al.* [1999] and *Zveryaev* [2002] which suggest a link between Indian Ocean SSTs and intraseasonal variability on decadal timescales or the studies by *Annamalai et al.* [2003] that have suggested a link between the equatorial waves associated with the MJOs and the potential triggering of the Indian Ocean Zonal Mode.

[7] The present study and line of research has been undertaken to try to answer some of the above questions. In regards to most of the questions highlighted above, it is important to emphasize that the character of atmospheric intraseasonal variability is strongly dependent on season. In austral summer, intraseasonal variability typically takes the form of the MJO which involves convective anomalies that propagate eastward from the Indian Ocean, across the Maritime Continent and western Pacific, and into the South Pacific Convergence Zone (SPCZ). In the boreal summer, intraseasonal convective events often propagate northeastward from the Indian Ocean across Southeast Asia, into the northwestern Tropical Pacific Ocean. Because of the significantly different nature of these two modes, and the different regions of the ocean they cross over, the answers to the above questions are likely to be dependent on season. This study deals with the austral summer case. We examine the boreal summer case in a separate study (D. E. Waliser et al., Indo-Pacific Ocean response to atmospheric intraseasonal variability: 2. Boreal summer and the intraseasonal oscillation, submitted to *Journal of Geophysical Research*, 2002). In addition, this study tends to focus mostly on the Indo-Pacific warm pool regions where the MJO-related forcing and associated ocean response is greatest, although some attention is given to the MJO's impact on the eastern Pacific Ocean. Because of the paucity of relevant ocean observations, particularly when considering ocean dynamics as well as a basin-wide perspective, the present study employs an ocean general circulation model (GCM) as the main tool for investigation. The model formulation is described in section 2. Section 3 describes the experimental setup, the procedures used to develop the MJO forcing conditions, and some validation analysis of the model's representation of intraseasonal variations. Section 4 describes the results and section 5 presents a brief summary of the results along with a discussion of their implications, the questions they raise and suggestions for future work.

2. Model

[8] The ocean GCM is the reduced gravity, primitive equation, sigma coordinate model of Gent and Cane [*Gent and Cane*, 1989]. The vertical structure of the ocean model consists of a mixed layer and 14 layers below according to a sigma coordinate [*Murtugudde et al.*, 1996]. The mixed layer depth and the thickness of the lowest sigma layer are computed prognostically and the remaining layers are computed diagnostically such that the ratio of each sigma layer to the total depth below the mixed layer is held to its prescribed value. The model employs the horizontal 'A' grid structure [*Arakawa and Lamb*, 1977] with a resolution of 1/3° latitude and 1/2° longitude. The model domain extends from 30°N to 30°S and from 32°E to 76°W. Fourth-order central differences are employed in the horizontal with second-order central differences in the vertical. The *Lorenz* [1971] N cycle scheme is used for time integration and a high-order, scale selective *Shapiro* [1970] filter provides horizontal friction. The model calendar year is composed of 360 days, and thus twelve 30-day months (or 72 5-day pentads).

[9] The model mixed layer is based on a hybrid vertical mixing scheme [*Chen et al.*, 1994] that combines the advantages of the traditional bulk mixed layer model of the *Kraus and Turner* [1967] type with the dynamic instability model of *Price et al.* [1986]. This allows simulation of all three major processes of oceanic vertical turbulent mixing; a) the bulk mixed layer model relates the atmospheric forcing to the mixed layer entrainment/detrainment, b) the gradient Richardson number mixing accounts for the shear flow instability, and c) an instantaneous adjustment simulates the high-frequency convection in the thermocline. Complete hydrology has been added to the model [*Murtugudde and Busalacchi*, 1998] with freshwater forcing treated as a natural boundary condition [*Huang*, 1993]. The UNESCO equation of state is used for computing buoyancy from salinity and temperature. A sponge layer is utilized at the north and south boundaries of the model domain, with the model damped toward the climatological values of *Levitus* [1994].

[10] Surface heat fluxes are computed by coupling the ocean GCM to an advective atmospheric mixed layer (AMLM) model [*Seager et al.*, 1995]. The improvements in tropical SST simulations and its feedback on model dynamics/thermodynamics associated with the incorporation of the AMLM are reported by *Murtugudde et al.* [1996]. Briefly, the model represents either a dry convective

layer or the mixed layer that underlies shallow marine clouds. Within the mixed layer, the air temperature and air humidity are determined by a balance between surface fluxes, horizontal advection by imposed winds, entrainment from above the mixed layer, horizontal diffusion and, for temperature, radiative cooling. Once the air temperature and humidity are determined, surface sensible and latent heat fluxes (and thus evaporation for the freshwater forcing) can be calculated in terms of the ocean model SST and the imposed winds. To compute the longwave radiative heat loss from the surface we use a standard bulk formula and observed cloud cover [*Seager and Blumenthal*, 1994]. Surface solar radiative forcing is taken from observed values estimated from satellite derived products. The specifics of each of the forcing data sets will be discussed in more detail in the next section. In summary, by using the AMLM, the net surface heat flux can be computed by specifying only the solar radiation, cloud cover and winds. These are all quantities that the ocean has only indirect control over and can be justifiably specified externally. The quantities that the ocean has some direct control over, i.e., air temperature and humidity, are modeled internally in terms of the SST, the surface winds, and the values of the wind, air temperature and air humidity at the continental margins. Note that in the model's standard configuration no heat flux correction is applied.

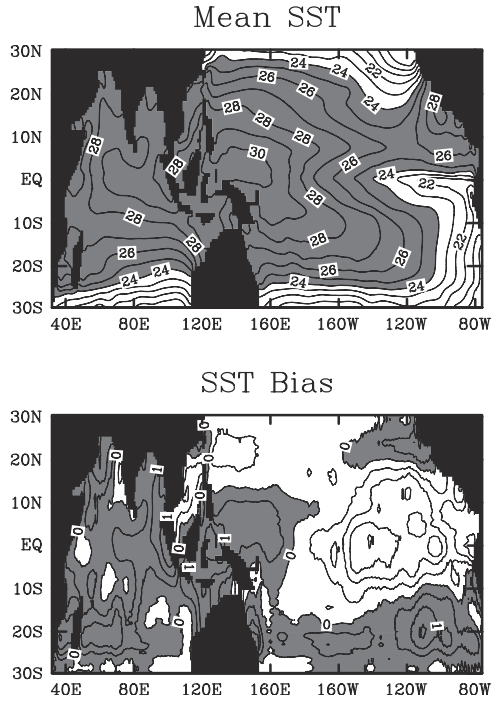

Figure 1. (top) Mean annual sea surface temperature (SST) from the ocean model. Contour interval is 1°C and shading starts at 24°C. (bottom) Difference between the model SST and observations [*Levitus*, 1994]. Contour interval is 0.5°C with positive values shaded.

3. Data and Experimental Setup

3.1. Climatological Forcing and Setup

[11] As discussed in the previous section, the surface forcing data required by the model consists of solar radiation, cloud cover, surface wind and stress, and the surface wind, air temperature and air humidity at the continental margins. Climatological surface solar forcing was obtained from the Earth Radiation Budget Experiment (ERBE) product of *Li and Leighton* [1993]. Climatological surface precipitation values were obtained from the satellite and in situ blended product of *Xie and Arkin* [1997]. Climatological cloud cover was obtained from the ISCCP-C "total cloud fraction" product of *Rossow and Schiffer* [1991]. Climatological values of near-surface air temperature and humidity at the model's continental margins were obtained from ECMWF (ERA-15) reanalysis. Climatological wind and wind stress values were obtained from SSM/I [*Atlas et al.*, 1996]. In the case of winds, the daily values of surface zonal and meridional wind from 1988 to 1999 were used to compute daily values of wind speed and wind stress. The latter used the standard bulk formula representation with the air density and exchange coefficient specified as 1.25 kg m^{-3} and 1.5×10^{-3}, respectively. The daily values were then used to compute mean 365-day annual cycles for each quantity that in turn were interpolated to 12-month annual cycles. Note that in order to account for wind gustiness which is not typically measured in satellite or sparse in situ data sets, a gustiness factor was incorporated by implementing a minimum wind speed threshold of 4 m s^{-1} directly into the climatological wind speed data set. The reason for applying this to the data itself rather than incorporating the threshold into the model code was so that anomalies in wind speed associated with the MJO could be added to the climatological values to produce intraseasonal fluctuations that included realistic low wind speed regimes [e.g., *Weller and Anderson*, 1996, Figure 9].

[12] Using the above climatological data sets as forcing, the model was integrated from an arbitrary initial condition for eighteen years, the last three of which were averaged to form the model climatology as well as to describe the model's internal variability, i.e., variability that arises from using only climatological forcing. Figure 1 illustrates the modeled and the difference between the modeled and observed [*Levitus*, 1994] mean SSTs. Apparent are the warm bias in the Indo-Pacific warm pool region and the cold bias in the eastern equatorial Pacific Ocean. This sort of bias structure is common in forced ocean model experiments that do not use specified air temperature and humidity values as boundary conditions as well as in coupled models. It is thought to be the result of deficient vertical mixing parameterizations in ocean models or poor stratus deck formulation in coupled models or both [*Delecluse et al.*, 1998; *Stockdale et al.*, 1998]. However, recent studies suggest that the cold bias in the cold tongue may be related in part to inaccurate representation of the radiative trapping by near surface phytoplankton blooms [*Murtugudde et al.*, 2002]. The SST errors in the Indo-Pacific warm pool are likely due to errors in surface radiative fluxes or winds or due to model deficiencies. Since the corrective fluxes required to remove these SST errors are nearly as large as the uncertainties in the fluxes, it is difficult to pinpoint the exact causes [see also *Seager et al.*, 1995; *Murtugudde et al.*, 1996]. Three aspects should be stressed regarding the model climatology, at least in terms of SST: 1) overall it is relatively realistic in terms of the large-scale structure, 2)

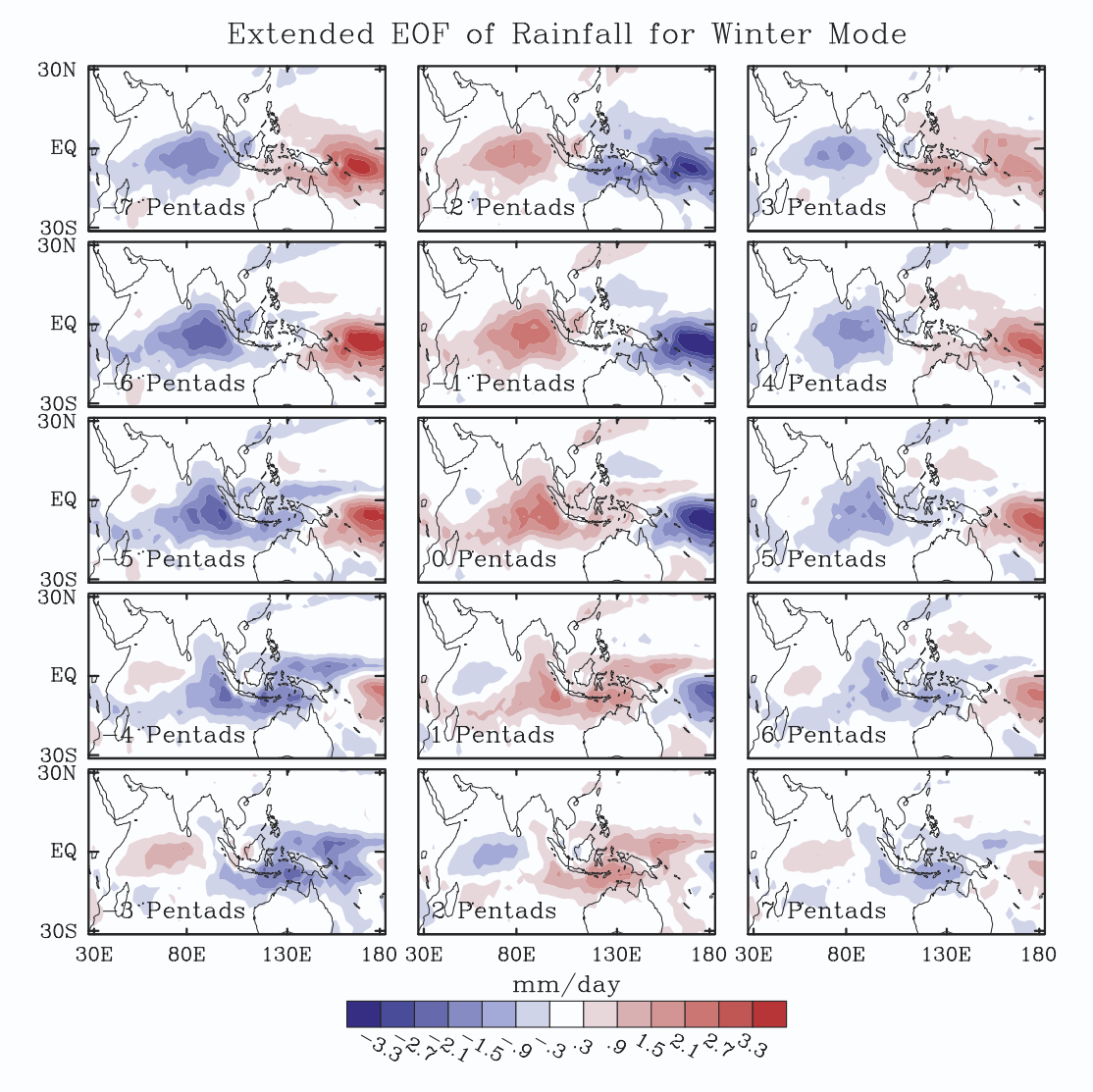

Figure 2. First mode extended empirical orthogonal function (EEOF) of filtered (35–95 days) Northern Hemisphere winter (November–April) rainfall for the tropical domain shown from the pentad values of *Xie and Arkin* [1997]. Time lags extend from −35 days (i.e., − pentads) in the upper left corner to +35 days (i.e., +7 pentads) in the lower right corner.

the present study relies primarily on the ocean model's anomalous response rather than on the climatological structure – albeit the two are not independent, and 3) sensitivity tests using an imposed flux bias correction to improve the near-surface climatology show that the main results of the study do not depend on the modest errors associated with the model's near-surface climatology. The latter aspect will be discussed in more detail in a later section.

3.2. MJO Forcing and Setup

[13] Ocean forcing conditions associated with the MJO were constructed using a compositing approach. MJO events were identified through extended EOF (EEOF) analysis of band-passed pentad (i.e., 5-day average) rainfall data [*Xie and Arkin*, 1997] that extends from 1979 to 1999. Band-pass filtering was performed using a 35–95 day Lanczos filter [*Duchon*, 1979]. In order to isolate the canonical form of the MJO, that which is most prevalent in boreal winter [*Wang and Rui*, 1990; *Hendon and Salby*, 1994; *Madden and Julian*, 1994], only Northern Hemisphere "winter" (hereafter, November–April) data were retained in the analysis. From these band-passed winter data, EEOFs are computed for ±7 pentad time lags on the region between 30°E and 180°E. Figure 2 shows that mode 1 pattern represents an eastward propagating structure with about a 50-day period that is strongly reminiscent of the MJO. Candidate events for constructing the MJO composite were selected when the value of the unit normalized amplitude time series of mode 1 exceeded 1.2. Figure 3 shows the amplitude time series of EEOF mode 1 along with the candidate MJO events. Also shown on Figure 3 are the temporal extents of the additional forcing data sets that are used for constructing the composite MJO forcing. These additional data sets include the: 1) daily SSM/I [*Atlas et al.*,

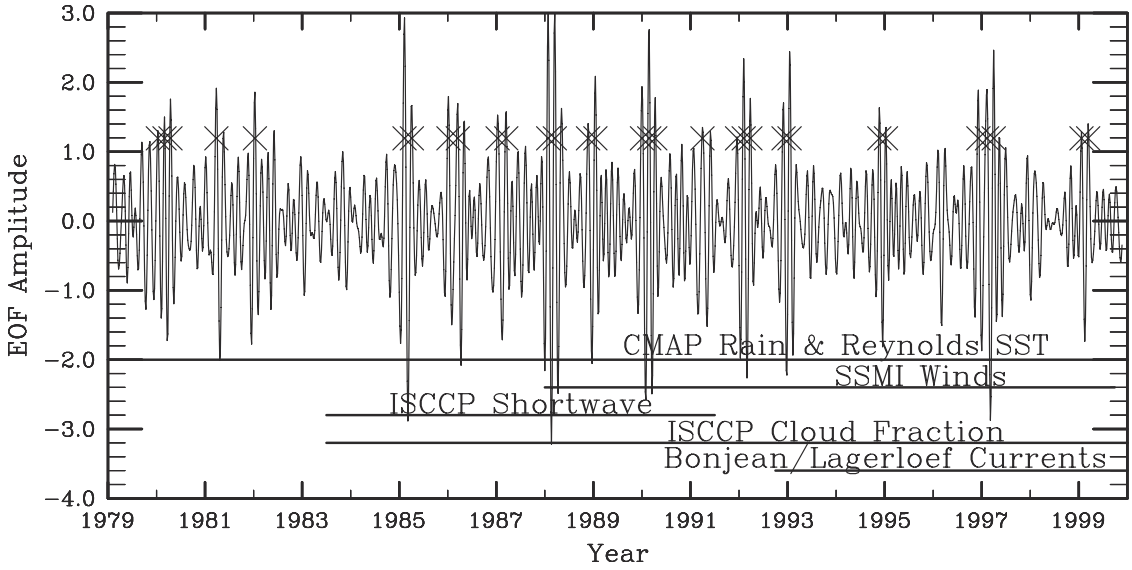

Figure 3. Amplitude time series for the first EEOF mode of filtered (35–95 days) Northern Hemisphere winter rainfall (see Figure 2). The X's represent MJO events selected for inclusion in the composite forcing. Horizontal lines and associated labels give the period encompassed by the given forcing and validation data sets. See section 3 for details.

1996] winds for computing wind speed, direction, and stress; 2) daily ISCCP-derived surface shortwave values [*Bishop et al.*, 1997]; and 3) daily ISCCP-D-derived total cloud fraction [*Rossow and Schiffer*, 1991]. In each case, these additional forcing data sets were interpolated to pentads (73/year) to match the temporal resolution of the rainfall data. Note that because of the nonoverlapping nature of the data sets, the shortwave composite, for example, contains fewer/different events than the wind composites. In addition, daily values of wind speed and wind stress were first computed from the daily values of vector wind. These daily values were then used to define the associated climatologies and in turn the anomalies.

[14] For each forcing data set, the corresponding candidate MJO events were averaged to form a composite forcing structure with the same lags as the EEOF (i.e., Figure 2). For rainfall, shortwave, cloud fraction and wind, this involved 31, 14, 19, and 19 events respectively. As expected and as seen in Figure 2, the above forcing structures exhibit a cyclic structure with a repeating timescale of about 50 days. For example, the map in Figure 2 with lag −25 days is nearly the same as the map with lag +25 days. Thus a complete MJO cycle, with a positive rainfall anomaly just beginning to form in the western Indian Ocean, can be constructed using the 10 pentads between −5 pentads lag to +4 pentads lag. In addition, to overcome the decrease in the magnitude of the forcing associated with averaging over different candidate events, the composite forcing fields are multiplied by a scale factor (in this case 1.7). This compositing procedure produces forcing fields required by the OGCM and that are associated with a "typical" MJO (see Figure 4).

[15] In general, the above compositing procedure is applied to the band-passed data for each forcing field. This helps to prevent interannual variability from biasing the MJO forcing fields. However, it is important to note that even though these composites are roughly cyclic and are constructed from (intraseasonally) band-passed data, there is no constraint imposed, from either the methods used here or the observed system, that the time mean of the composites be zero at any given spatial location. For example, the convective phase of a typical MJO may involve slightly more westerly wind or a greater positive rainfall anomaly than occurs in the opposite sense for the subsidence phase. If this were the case, the balance would be made up during all the intervening periods between MJO events to give a zero anomaly for the total time series. The approach described above is an attempt to capture MJO event forcing conditions that are typical, realistic and ultimately based on observations. Examination of the composite MJO forcing shows that in fact they do exhibit small time mean values. These values are referred to as "residual" means and sensitivity tests to determine their impact are discussed below. However, it is important to emphasize that this study is concerned with the ocean response to MJO conditions/events, not those associated with forcing from intervening periods. Composite forcing fields were also constructed using the unfiltered anomaly data. Not surprisingly, these anomaly based composites did exhibit nontrivial time mean values (i.e., "residual" mean) values that arose from the interannual (i.e., ENSO) variability within the data records. Thus these anomaly based composites were not used to represent MJO forcing but rather to provide a point of comparison for evaluating and describing the composites based on the filtered data.

[16] Since a number of MJO events often appear in sequence (e.g., Figure 3), the composite event can be concatenated together to form an idealized sequence of MJO events. However, it should be kept in mind that because the timescale of the MJO and the length of the period of the year when the canonical form of the MJO is most strongly exhibited (∼November–April), only about

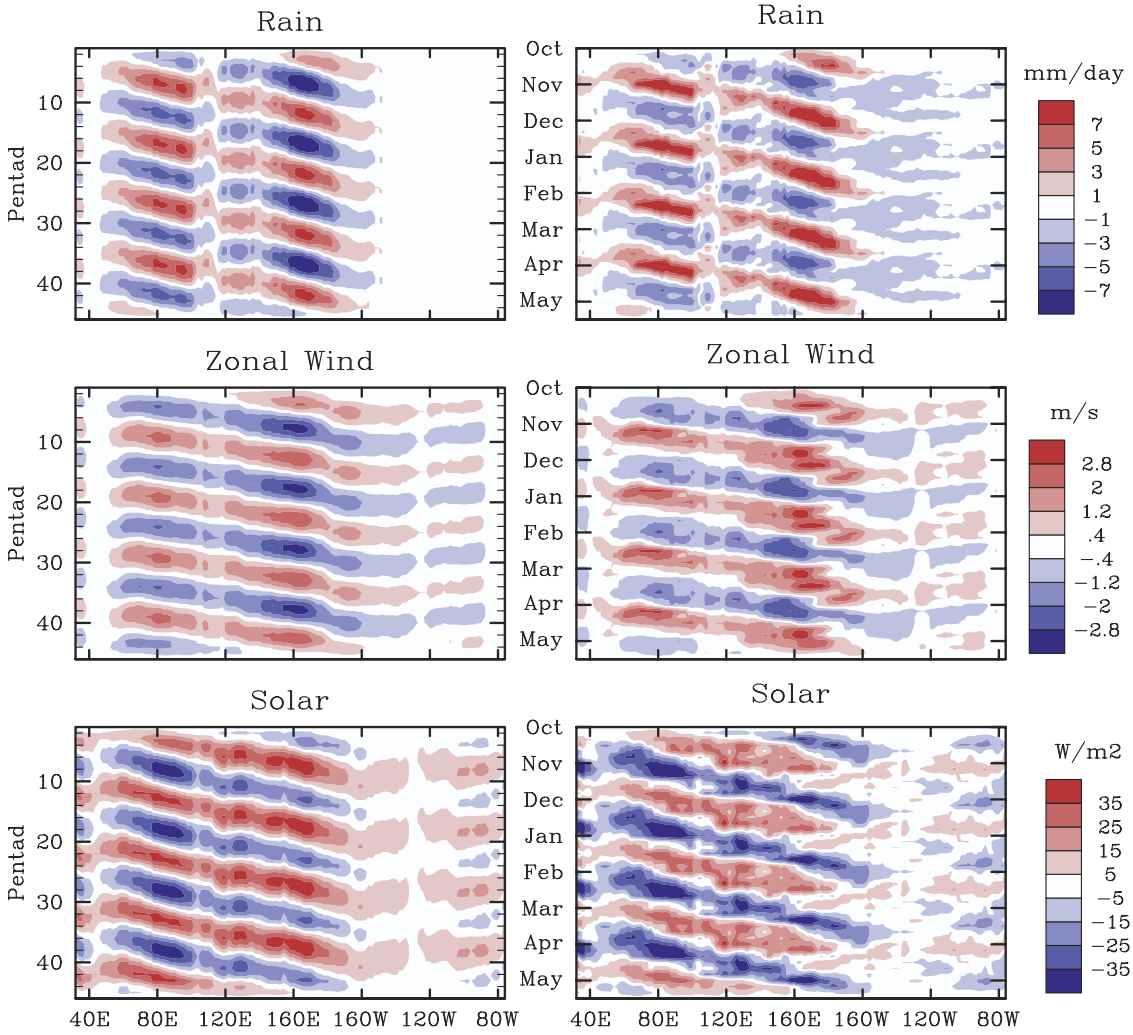

Figure 4. Equatorial (3°N–7°S) time-longitude diagrams of ocean model forcing fields associated with a sequence of four canonical MJO events produced from composites of (left) band-passed (35–95 days) and (right) total anomaly (top) rainfall, (middle) zonal wind, and (bottom) surface shortwave radiation. Note that the *y* axis labels are given both in terms of pentads and calendar year when the anomalous forcing is applied.

3–4 events can be expected to occur in any given winter. Figure 4 illustrates a sequence of four composite MJO events in terms of rainfall, zonal wind, and surface shortwave. The temporal extent of the composite sequence is 230 days (=46 pentads); this includes four 10-pentad MJO cycles plus 3 pentads at the beginning (end) of the sequence which contain 0, 1/3, and 2/3 (2/3, 1/3, and 0) times the first (last) perturbation value. The panels on the left show composite events that were constructed from band-passed data while those on the right show composites constructed from anomaly (i.e., unfiltered) data. Note that the significant similarity between the band-passed and anomaly composites illustrates that the intraseasonal timescale of the phenomena is exhibited naturally in the data and not imposed by the band-pass operation. The analogous diagrams for wind stress and speed (not shown) look very similar to the zonal wind diagram with minima and maxima on the order ±0.5 dyne cm^{-2} and ±2 m s^{-1}. Similarly, the diagram for cloud fraction closely resembles the rainfall diagram but with minima and maxima of about ±0.25. To illustrate that the magnitude and character of the composite structure are reminiscent of observed events, Figure 5 shows pentad anomaly and band-passed rainfall data from the equatorial Indian and western Pacific Oceans for three winter periods (1988, 1989, and 1997), along with the corresponding data from the composite MJO (i.e., Figure 4). A comparison of these plots demonstrates that the amplitude of the composite events (and thus the use of the above scale factor) is typical of observed events and that the constructed sequence of events is not too dissimilar from what is exhibited by the observations.

[17] To succinctly illustrate the spatial variability associated with the MJO forcing, Figure 6 shows the standard deviation of the composite MJO based on band-passed data. The analogous patterns associated with composites based on anomaly data (not shown) are nearly the same except the magnitude is increased by about 10–15%. This, as well as the comparisons above between the

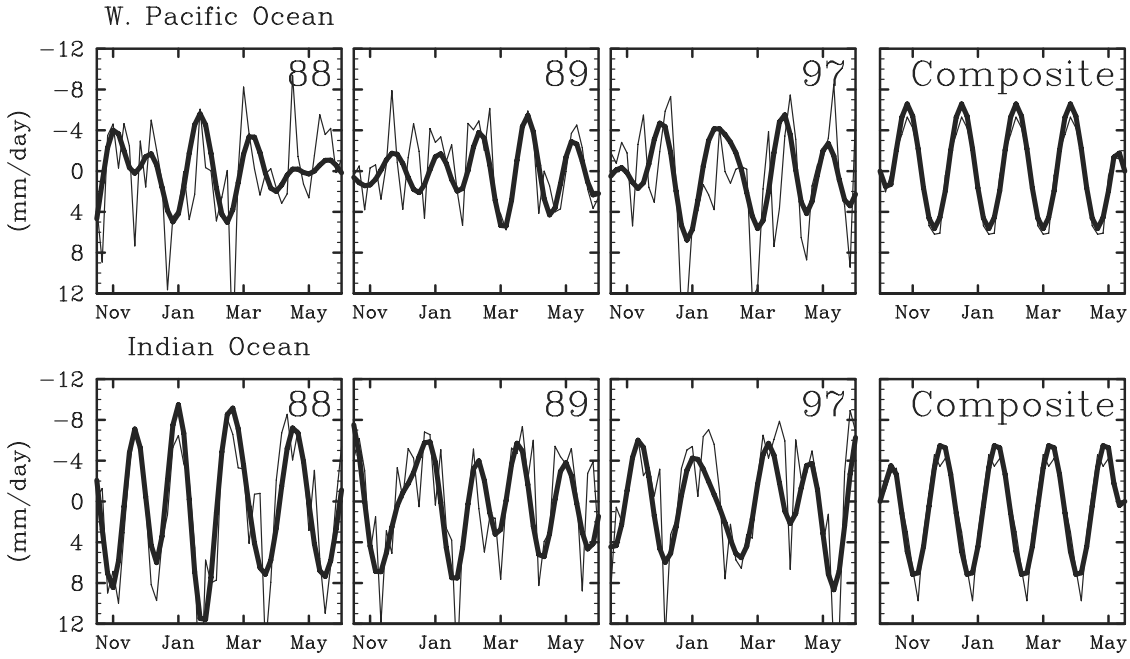

Figure 5. (leftmost three panels) Band-passed (35–95 days; thick) and total pentad (thin) rainfall anomalies for three Northern Hemisphere winter periods (1988, 1989, and 1997) over the (top) near-equatorial western Pacific (3°N–7°S; 150°E–160°E) and (bottom) central Indian (3°N–7°S; 90°E–100°E) Oceans. (right) Sequence of four canonical MJO events produced from composites of band-passed (thick) and total anomaly (thin) rainfall data.

band-passed and anomaly composites, indicates that the use of band-pass filtering to construct the MJO forcing had the desired effect of limiting the potential for interannual bias, but did not impose a timescale artificially or significantly change the spatial structure or magnitude of the variability. The maps in Figure 6 provide an indication of the regions where one would expect to find a local ocean response to the imposed MJO forcing. Note that because of the seasonal influences on the MJO, most of the forcing maxima are contained between about 5°N and 15°S, with the zonal wind stress and wind speed more tightly confined than the forcing associated with clouds and precipitation. In addition, it is worth noting that there is relatively high wind stress variability in several regions of the subtropics as well. We will present similar figures associated with the ocean response to illustrate the mapping between the atmospheric forcing and the ocean response for the intraseasonal timescale.

[18] For the MJO simulations described in this study, the perturbation forcing fields associated with the composites were added to the climatological forcing fields and then used to force the ocean model. The perturbations were added such that the MJO forcing illustrated by Figure 4 begins on 1 October. From 1 October the simulations were integrated for one year. In such a case, the MJO is active between October and late-May (i.e., 46-pentads), after which the forcing returns to its climatological values. The ocean response to intraseasonal forcing was then measured and described by the difference between the simulations with MJO forcing and the simulations using only climatological forcing. Note that for the case of the wind speed, the perturbation from the composite is added to the climatological forcing without an additional application of the low wind speed threshold (see section 3a). Thus for the suppressed (wind speed) phase of MJO, the total wind speed can and does fall below the 4 m s^{-1} threshold that was applied to the climatological forcing [cf. *Weller and Anderson*, 1996, Figure 9]. Given the 4 m s^{-1} threshold in the climatology and the size of the composite MJO wind fluctuations, the wind speed rarely falls below 2 m s^{-1} and never below 1.1 m s^{-1}. These very low wind speed cases (<2 m s^{-1}) occur in a few locations (~10 2° × 2° model forcing grid points) over the course of 1–2 pentads during the low wind speed phase of the composite (10-pentad) MJO cycle in a small region between 140°–160°E and 0–10°S. In addition to the MJO simulation that utilizes all the forcing fields, hereafter referred to as the control, simulations were also performed that excluded one or more forcing fields. These additional simulations were performed to help diagnose the forcing mechanisms and associated processes responsible for various features in the simulated ocean response.

3.3. Validation Data and Methods

[19] To demonstrate that the model has a realistic representation of the near-surface ocean response to intraseasonal forcing it is useful to compare the model response to the observed response using anomalous forcing from a relatively active MJO period. Data sets useful for validation of the large-scale ocean response include the weekly SST estimates of *Reynolds and Smith* [1994] and the surface current estimates of *Bonjean and Lagerloef* [2002]. Note that the latter contains data only for the Pacific Ocean. The

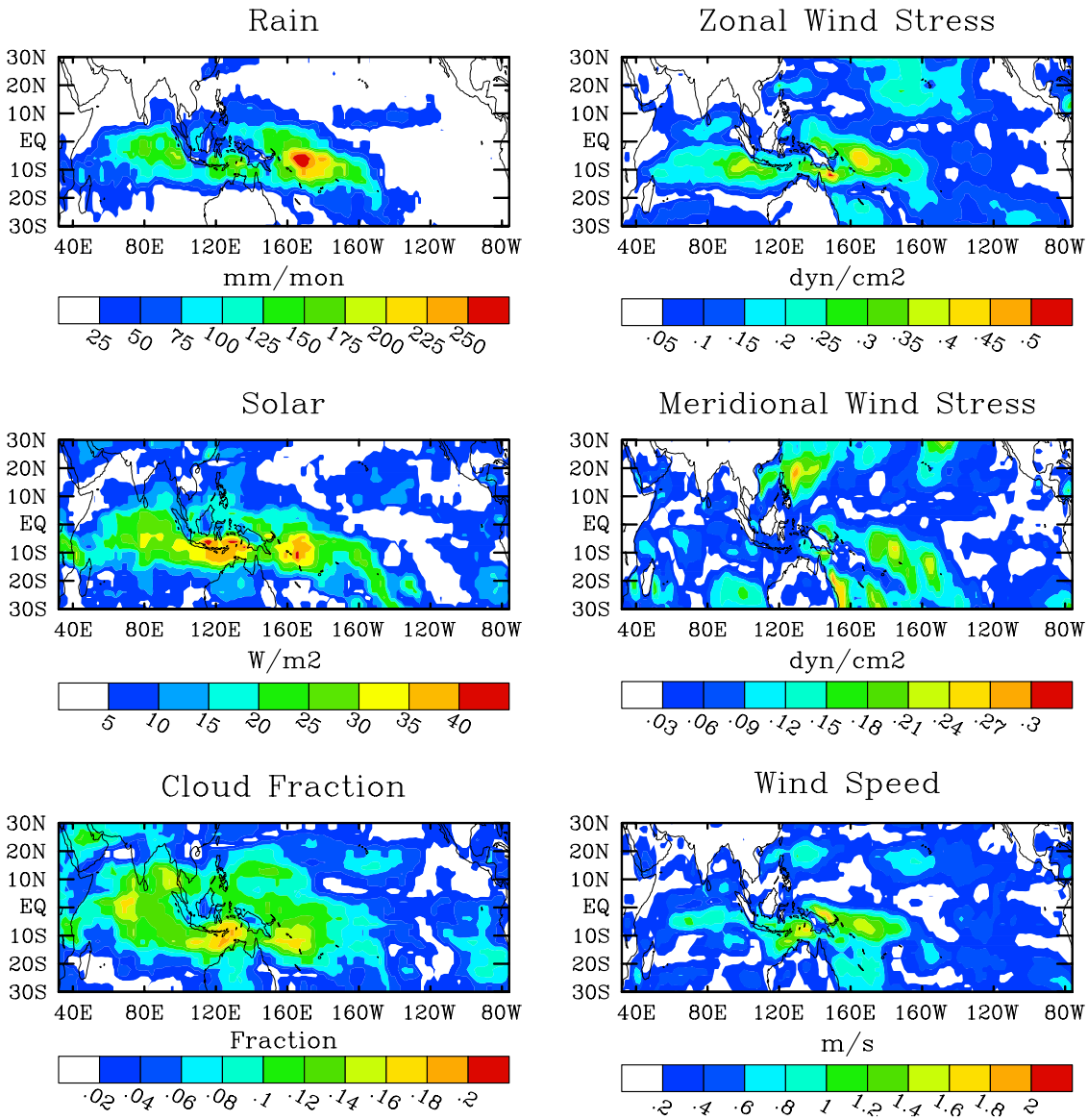

Figure 6. Standard deviation of the composite MJO forcing fields produced from band-passed (35–95 days) data. See section 3b.

periods covered by these data sets are indicated on Figure 3. Unfortunately there is no overlap between the surface current data set and surface shortwave data set, which is a necessary forcing field of the model. However, because of the excellent field-to-field relationship between precipitation and shortwave perturbations on the intraseasonal timescale (e.g., Figure 4), an estimate of the band-passed surface shortwave values was derived from the precipitation and cloud fraction data using the canonical correlation analysis (CCA) approach described by *Waliser et al.* [1994]. Briefly, EOFs of a combined field made up of the overlapping band-passed precipitation and cloud fraction data as well as the band-passed shortwave data were computed, and then CCA was performed on the period the two data sets overlap (i.e., July 1983 to June 1991). This allows the construction of an empirical model to relate precipitation and cloud fields to the shortwave field. The first 8 modes were found to be significant at the 99.9% level and thus were used for the model estimate of shortwave; their eigenvalues (i.e., correlations) ranged from 0.97 to 0.50. The number of degrees of freedom ($N \sim 50$) was determined from the length of the shortwave data set (~8 years) and the characteristic timescale of the MJO (~7/year). Figure 7 shows the spatial correlation maps of the model estimate of band-passed shortwave with the observed values over the entire period of overlap (top). Also shown are the correlation (middle) and root mean square difference (bottom) maps between the band-passed composites based on the original data and the model estimated data. These latter two maps were calculated using only the independent model derived data (i.e., data after July 1991). The good agreement between these fields, particularly in the region of strong variability (Figure 6) demonstrates that there is a fairly robust relationship between the large-scale low-frequency variations of

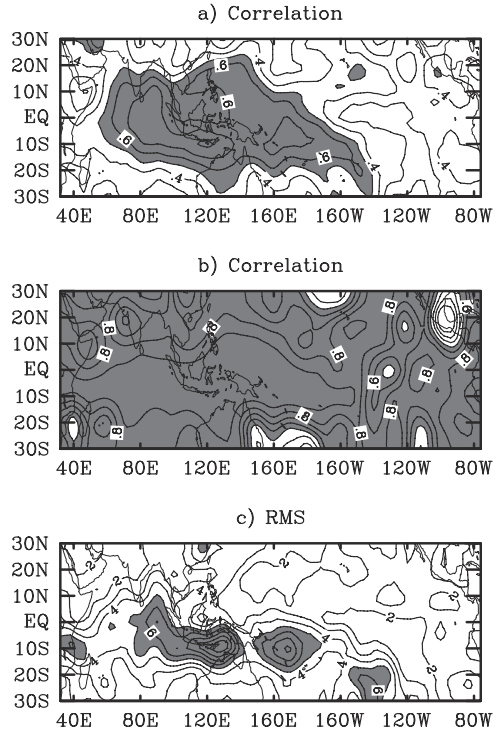

Figure 7. (a) Correlation map of the CCA-based model estimate of intraseasonal shortwave anomaly with the observed values over the entire period of overlap (July 1983 to June 1991; see Figure 3). (b) Correlation and (c) root mean square difference maps between the band-passed composite shortwave based on the observed data (July 1983 to June 1991; see Figures 4 and 6) versus a composite based on the model estimate over the period July 1991 to December 1999. Contour interval for both Figures 7a and 7b is 0.1 with shading starting at 0.5. Contour interval for Figure 7c is 1 Wm^{-2} with shading starting at 5 Wm^{-2}.

precipitation and clouds and the shortwave that can be rather easily modeled [e.g., *Waliser et al.*, 1994; *Shinoda and Hendon*, 1998].

[20] Utilizing the above modeled version of intraseasonal shortwave variations, along with the observed wind, cloud fraction and precipitation band-passed data, a simulation was performed with ''observed'' intraseasonal forcing for the period 1994 through 1999. Figure 8 shows a comparison between the (band-passed) observed SST and zonal surface current (left) along with the modeled values (right) for the equatorial region during the winter of 1996/1997 (see Figure 3). The SST shows rather good agreement during periods throughout this entire period, particularly west of about 160°W. Because of the chaotic nature of tropical instability waves (TIWs), little agreement would be expected in the eastern equatorial Pacific Ocean, particularly in SST. While there is still fair agreement between the modeled and ''observed'' zonal current, it is not as good as with the SST. The magnitude is slightly greater in the model and the anomalies are more coherent in space and time. This can at least partly be ascribed to the sampling associated with the Bonjean and Lagerloef currents that are based in part on satellite-derived sea level observations. These observations typically only sample any given point in the equatorial band about every 10 days. This is marginally adequate to get a sense of the intraseasonal variability but clearly not sufficient to provide a robust representation. Even so, the modeled and observed values do exhibit a good deal of similarity. This modest agreement, along with the SST comparison above, as well as previous uses of the same basic model to analyze the intraseasonal timescale [e.g., *Shinoda and Hendon*, 2001] demonstrate that the model exhibits a fair amount of fidelity at simulating the ocean response to intraseasonal forcing.

4. Results

4.1. Basin-Wide Ocean Response

[21] In order to begin to describe the overall basin-wide response to MJO forcing, an estimate of internal model variability (i.e., when only forced by annual cycle forcing) is shown in Figure 9. Figure 10 shows the added model variability that is forced by the MJO. To construct the maps in Figure 9, the variances about the mean annual climatology were computed from the same 3-year period used to construct the climatology (see section 3a). The average variance was then computed for the October through late-May period (=46 pentads). This variability is only associated with climatological forcing and thus can be ascribed to internal variability mechanisms in the model (e.g., TIW). To construct the maps in Figure 10, the anomalous response of the model was first determined by computing the differences between the MJO forcing case and the climatology. Then the variance of the anomalous response over the forcing period (October to late-May) was computed. This variability contains both MJO forced variability and model internal variability. To estimate the part associated with the MJO forcing, the background variability described above was subtracted from this quantity. For both Figures 9 and 10, the variance quantity is shown in terms of standard deviations.

[22] From Figure 9, it is evident that the internal variability of the model, as described by this estimate and exhibited during this time of year (October to late May) is almost exclusively limited to the equatorial Pacific. In these regions SST, current, sea level, mixed-layer depth and salinity variations are on the order 0.4 C, 20 cm/s, 4 cm, 5 m, and 0.05 PSU. This variability is a result of the model's simulated TIWs. Examination of maps analogous to those in Figure 9 for the surface heat budget terms show that the internal SST variability that occurs in the equatorial Pacific is primarily a response to variations in zonal and meridional advection ($\sim <= 150$ Wm^{-2}), with modest contributions from vertical advection. ($\sim <= 40$ Wm^{-2}). Vertical entrainment and surface heat fluxes make only minor contributions ($\sim <= 15$ Wm^{-2}), the latter of which results from the dependence of the turbulent and longwave fluxes on the model's SST itself. The internal variability exhibited in model sea level, and to some extent in salinity, appears to be associated with Rossby wave adjustments resulting from the TIW activity.

[23] The maps in Figure 10 illustrate a rather wide range of influences associated with the added MJO forcing. The SST exhibits additional variability on the order of 0.3°–0.5°C in the equatorial Indian and western Pacific Ocean

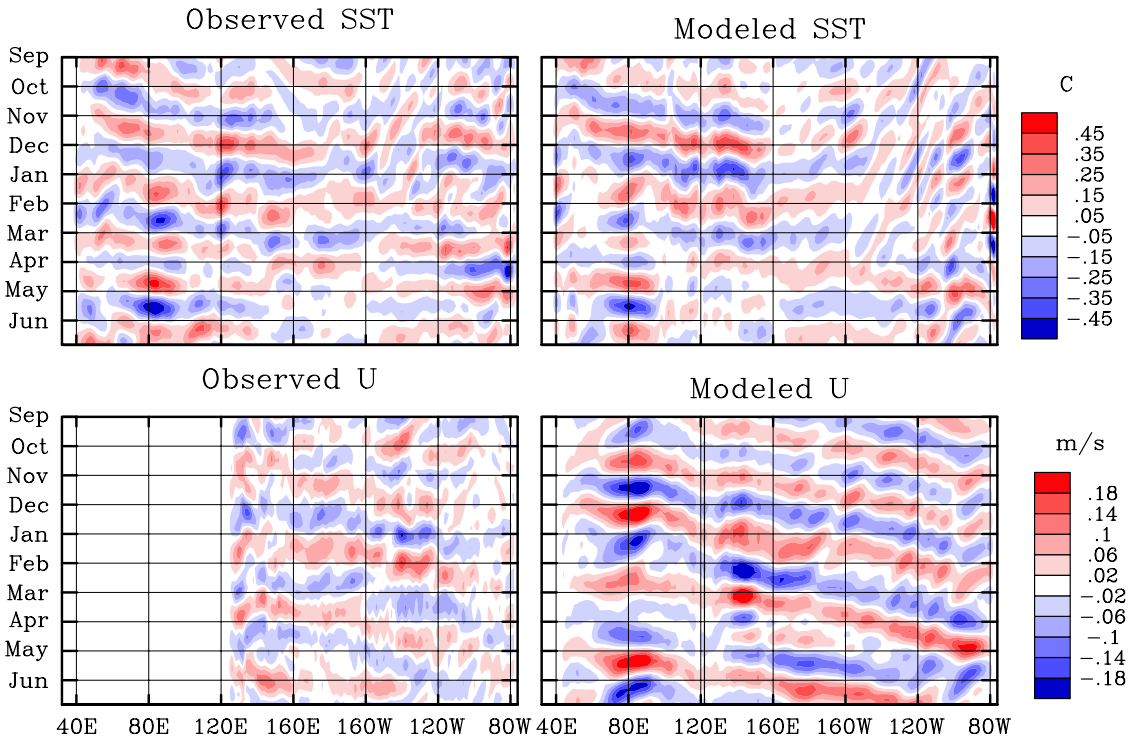

Figure 8. Equatorial (5°N–10°S) time-longitude diagrams of (top) intraseasonal SST [i.e., *Reynolds and Smith*, 1994] and (bottom) zonal current variations from observations [*Bonjean and Lagerloef*, 2002] and the model. The "Observed U" has had a 3-point box filter (2° longitude per point) applied in the longitudinal direction.

sectors that is concomitant with the areas of largest local convection and wind forcing. More specifically, SST variations in this region appear to be driven by comparable variability in horizontal and vertical advection (~10–15 Wm^{-2}), with larger contributions from surface heat fluxes (~25–40 Wm^{-2}), mainly shortwave and latent heat flux. The characteristics of the SST response and associated forcing mechanisms, in this as well as other locations, will be discussed in more detail below. Apart from the Indo-Pacific region, there is strong forced variability exhibited in the far eastern Pacific Ocean and an additional area of weak variability in the northwestern Tropical Pacific. The former is primarily driven by enhanced variability in meridional advection and to a lesser extent net surface heat flux and vertical and zonal advection. The latter is driven almost exclusively by wind speed induced (see Figure 6) latent heat flux anomalies (~ <= 30 Wm^{-2}) and to a lesser extent solar variations (~ <= 15 Wm^{-2}). This eastern and northwestern Pacific SST variability indicates that the ocean response to canonical MJO forcing would typically include systematic variability remote from the main forcing region as well as the expected variability in the Indo-Pacific equatorial regions.

[24] Mixed layer depth (MLD) variability associated with the added MJO forcing extends over a fairly comprehensive area of the tropical Indian and Pacific basins. In the equatorial Indian and western Pacific Oceans, the variability brought about by the MJO forcing is about 5–15 m (in terms of standard deviation), which is similar to what was found for the TOGA COARE IOP [*Anderson et al.*, 1996]. The manner these variations are related to the forcing will be described in more detail below. Apart from the equatorial Indo-Pacific region, there are other areas with similar size variability where the local MJO forcing is considerably less (e.g., subtropics, eastern/central Pacific). These are regions that tend to exhibit a fair amount of wind variability (Figure 6), and thus the MLD variability is associated with wind-induced mixing. Supporting evidence for this comes from simulations performed with the anomalous wind stress forcing excluded, MLD variations only occur in the equatorial Indian and western Pacific Oceans. While the typical MLD variations between the above domains are of a similar size, they are much smaller (larger) relative to the mean values in the subtropical (tropical) areas where typical mixed layer depths are on the order of 60–100 m (20–40 m). Thus the impact that these MLD variations might have on SST or salinity would be expected to be much smaller in the subtropical areas. The salinity variability associated with the MJO forcing occurs almost exclusively in the equatorial Indian and western Pacific Ocean, except for a relatively small region in the eastern equatorial Pacific. The former is driven by latent heat flux and precipitation variability while the latter is associated mainly with meridional advection that comes about through the slight enhancements in TIW activity. In any case, these salinity variations are very small given that the model's mean salinity ranges from about 35.1 to 34.0 psu across the entire equatorial domain.

[25] Dynamic variability associated with the added MJO forcing is strongly constrained to the near-equatorial latitudes. This is expected given the spatial and temporal scales

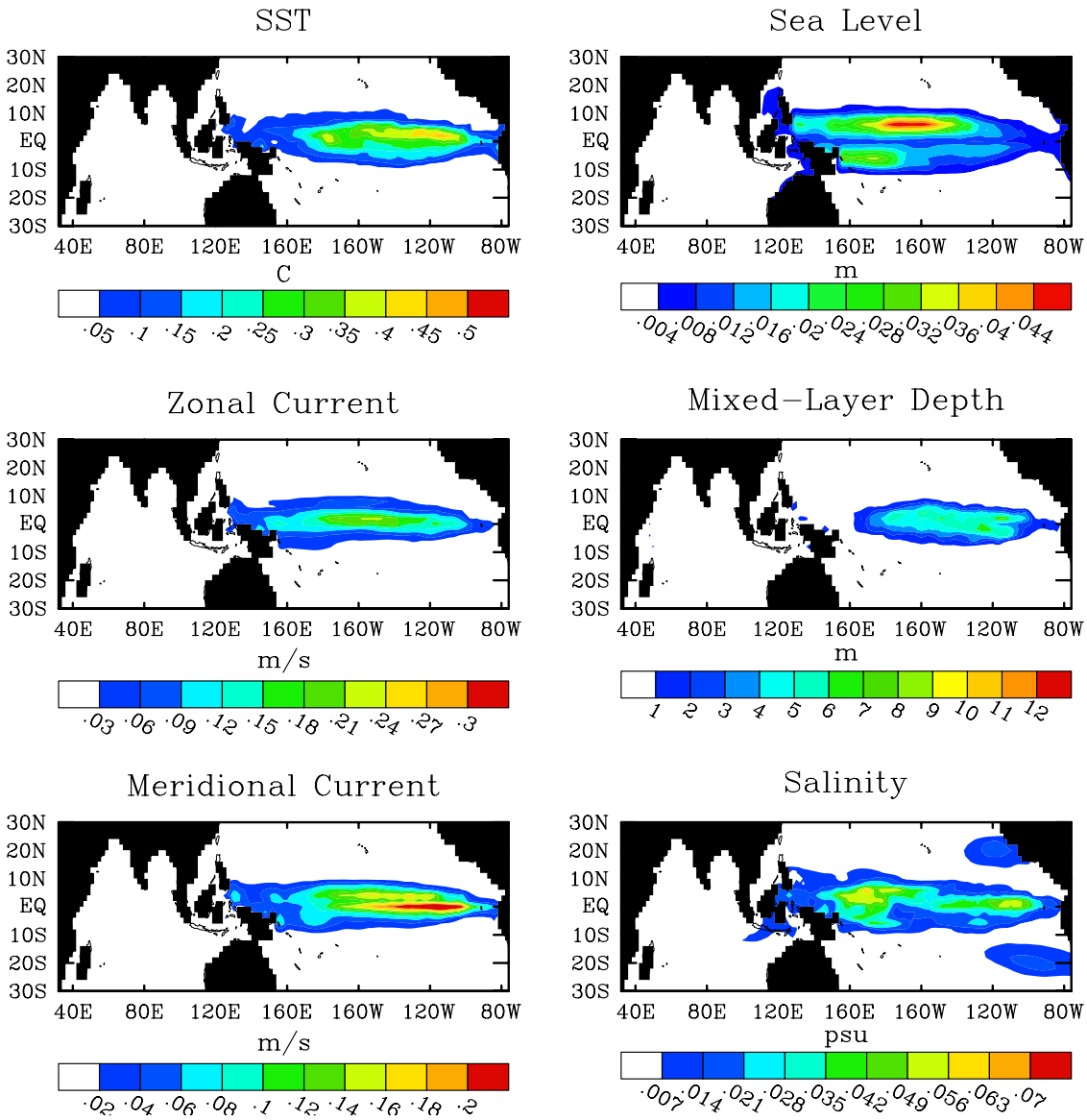

Figure 9. Estimate of internal model variability (shown in terms of standard deviations) that results only from annual cycle forcing. Variances were computed using the October through late-May departures from the mean annual climatology for the same 3-year period used to construct the model's annually varying climatology (see sections 3a and 4a).

of the forcing and equatorial wave dynamics [e.g., *Matsuno*, 1966; *Cane*, 1979]. Apart from the direct ocean response in the Indian and western Pacific Ocean, which involves variability in surface zonal and meridional current on the order of 30 cm s^{-1} and 10 cm s^{-1}, respectively, there is added variability in the eastern Pacific associated with both enhanced TIW activity as well as the impacts from remotely forced equatorial Kelvin wave activity. The presence of these latter processes will become more apparent from the discussion below. However, the stark difference between the internally generated sea level variability in Figure 9 and the variability associated with the added MJO forcing in Figure 10 depict a process in the ocean response to MJO forcing that is not present in the internal variability, namely Kelvin wave activity. In addition, the presence of sea level variations extending poleward on the eastern side of each basin further supports the presence of this type of equatorial wave activity.

4.2. Detailed Ocean Response and Associated Processes

[26] Figures 11 and 12 show the space time evolution of the (composite) ocean model response, in terms of SST, MLD, and surface current, to the applied MJO forcing. The composites were computed by averaging the model response over the four MJO events (i.e., Figure 4). The convention for the time lag shown in each panel of the figures is based on the canonical MJO rainfall pattern shown in Figure 2. Thus, on the basis of the discussion in section 3b, each MJO event cycles through pentads −5 to +4 of the rainfall structure shown in Figure 2. The four panel sequences shown in Figures 11 and 12 correspond to lags −3, −0.5, +2, and +4.5 (meaning an average between +4 and −5 pentads) pentads.

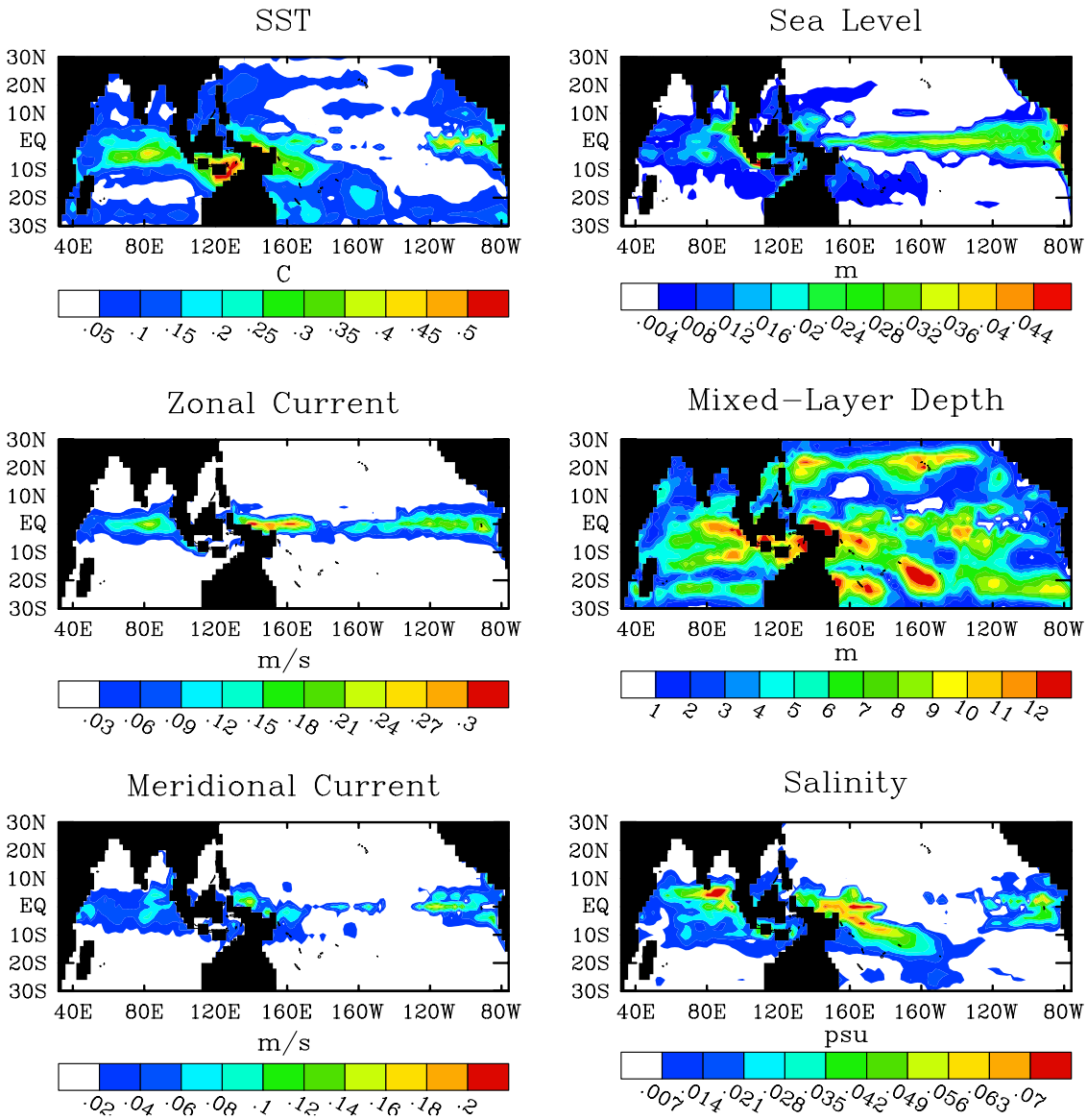

Figure 10. Estimate of the ocean model's response to MJO forcing, shown in terms of standard deviation. Values were calculated by first computing the differences between the MJO forcing case and the climatology. The variance of these differences (i.e., anomalous response) over the forcing period (October to late-May) was computed, and then the result associated with the internal variability (i.e., Figure 9) was subtracted from this quantity.

These figures show that for the most part, the SST evolution through the equatorial Indian and western Pacific Oceans is as expected (see studies cited in the Introduction). While there is significantly less observational data available for MLD and surface currents in this region, the evolution of these quantities is also not inconsistent with expectations. The MLD tends to shoal (deepen) about 5–10 (10–20) m during warm, low wind (cool, high wind) periods, and the equatorial zonal (meridional) surface currents oscillate between westward (divergent) and eastward (convergent) anomalies with a magnitude on the order of 30 (10) cm s^{-1}. A more detailed and complementary picture of the evolution of the ocean response in these regions is shown in Figures 13 and 14. Figure 13 is based on a location near the equator in the central Indian Ocean. Figure 14 is based on a small ocean domain within the Maritime continent region. The forcing is shown in Figures 13a and 14a, the response in terms of SST and MLD is shown Figures 13b and 14b, the main contributing elements to the mixed layer heat budget are shown in Figures 13c and 14c, and finally, the components of the surface heat flux are shown Figures 13d and 14d. In the case of the Figures 13c, 14c, 13d, and 14d, positive values indicate surface warming. Note that consistent with the discussion of "residual" mean forcing in section 3b, the time mean of the forcing data shown in Figures 13a–16a are not necessarily exactly equal to zero.

[27] With respect to the central Indian Ocean region, the main elements of the forcing are derived from surface wind variations that impact the latent heat flux and advection terms, and the rainfall and clouds that impact the surface

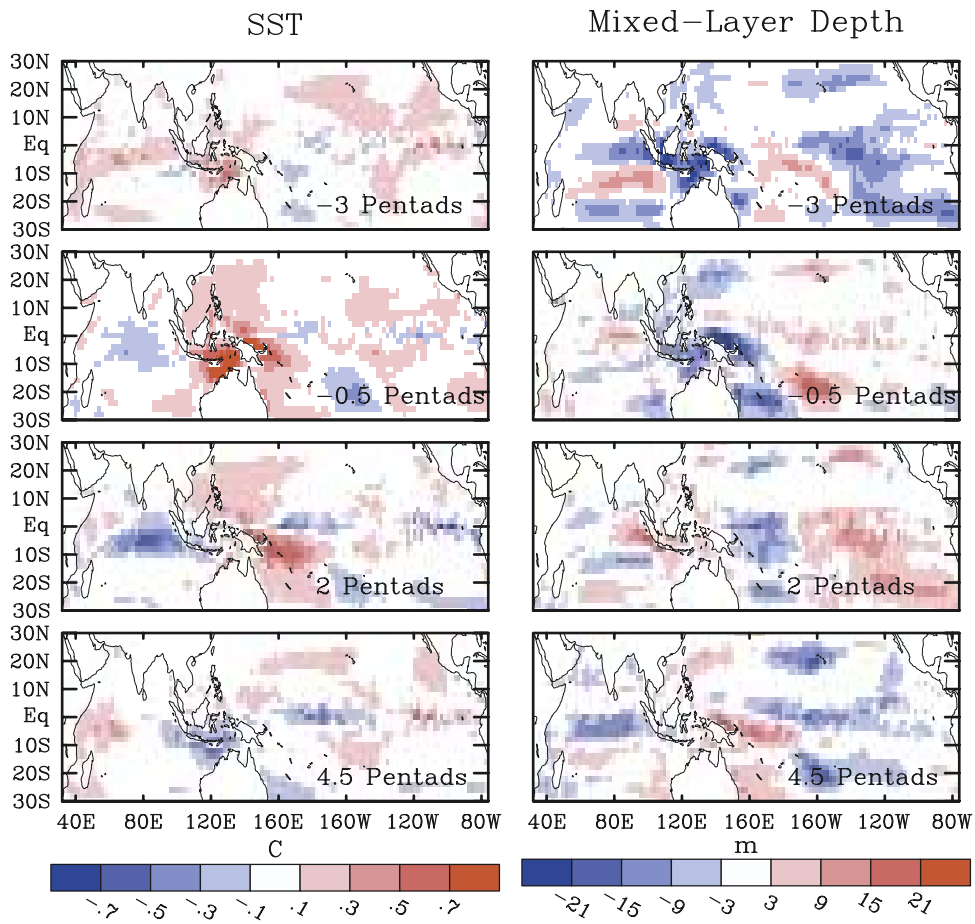

Figure 11. Composite ocean model response in terms of (left) SST and (right) mixed layer depth. The composites are computed by averaging the model response, at a given time lag relative to the MJO forcing, over the four MJO forcing events (i.e., Figure 4). The convention for the time lag, which is given in the lower right in each map, is based on the canonical MJO precipitation pattern shown in Figure 3. Note that a lag of −3 pentads occurs within the calendar year forcing at October P6, December P4, February P2, and March P6, where Pn is the pentad number for the given month. For lag −0.5 pentads the dates are November P2.5, January P0.5, February P4.5, and April P2.5. For lag 2 pentads the dates are November P5, January P3, March P1, and April P5. For lag 4.5 pentads the dates are December P1.5, January P5.5, March P3.5, and May P1.5, and October 3.5.

shortwave. In this region, during this time of year, the zonal wind anomalies tend to determine the phase of the wind speed anomalies relative to the MJO event which in turn determines the phase of the latent heat flux, the second largest term in the surface heat flux budget. Given that the peak in surface rainfall slightly precedes the peak in cloudiness [cf. *Myers and Waliser*, 2003] and the peak in wind speed lags slightly behind the minimum in latent heat flux (because of the effects from SST), positive anomalies of latent heat and shortwave flux are in phase and act together to heat and cool the ocean surface. The variations in net longwave, which are considerably smaller, are out of phase with the shortwave and latent heat flux given that clouds increase the downward component of longwave radiation. The "Qnet-Sum" term depicts the amount of shortwave energy lost out the bottom of the mixed layer. This term tends to be out of phase with the shortwave and latent heat flux because of the behavior of the MLD. Further, it tends to only exhibit negative values and these occur during periods of strong mixed layer shoaling; during other times the MLD is sufficiently deep (∼40 m) to capture nearly all the shortwave energy.

[28] In summary, it can be seen that for this location that the SST variations are primarily driven by surface heat flux, namely the evaporation and shortwave, and to a lesser extent net longwave, although the vertical and meridional advection do appear to contribute in some instances. These results are not inconsistent with the results of *Shinoda and Hendon* [1998] which showed general agreement between the observed SST and results from a mixed layer model forced with estimates of observed forcing. However, their results showed departures between the model and observed data (their Figure 3) large enough to suggest that dynamic processes might play a nontrivial role during some times and at some locations. The results from the present experiments suggest that the warming and cooling associated with

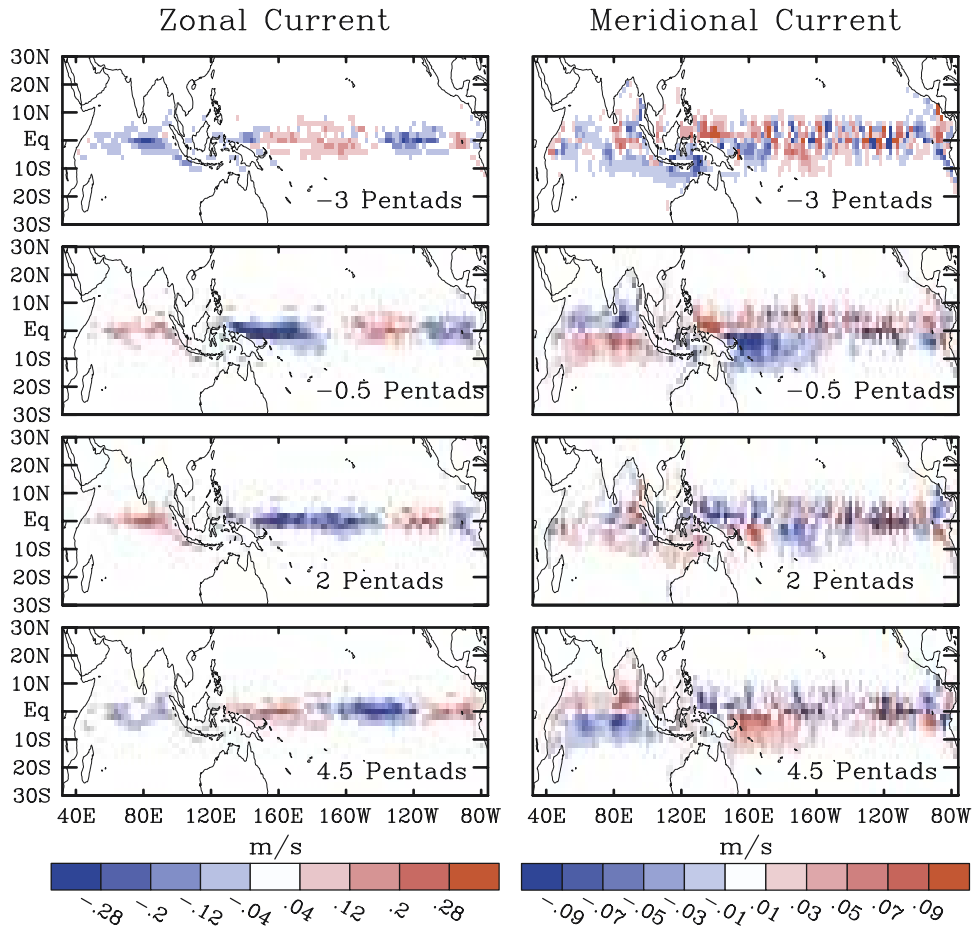

Figure 12. Same as Figure 11, except for surface (left) zonal and (right) meridional current.

vertical and meridional advection can be as large as 50% of the size of the net surface heat flux variations. However, the following contrast between the two is important to note. The phase of the vertical heat advection exhibits a rather systematic lag relative to the MJO forcing. Specifically, it lags about 1/4–1/2 cycle behind the zonal wind anomaly. In contrast to the vertical advection, and certainly the other forcing terms mentioned above, the contribution from the meridional advection does not occur in as systematic of fashion relative to the phase of the MJO. This suggests the presence of transient wave effects influencing the response. Since the meridional current is strongly affected by Rossby and Rossby gravity waves, the changing nature of the meridional advection may be related to remote production of such waves at the eastern boundary via reflection of equatorial Kelvin waves. In addition, it should be noted that the anomalous forcing associated with the wind stress curl might also play a role in the evolving nature of the SST response in this region; this will be discussed in more detail in section 4d. While the above model results support the notion that much of the intraseasonal SST variability is associated with surface heat flux variations, they also illustrate that for the central Indian Ocean mixed layer dynamics and three-dimensional ocean processes are likely to be important to accurately represent the evolution of SST during MJO events. In contrast to the central Indian Ocean, dynamical processes appear to play very little role in the evolution of the SST around the Maritime continent (Figure 14). Certainly variations in mixed layer depth (~25–60 m) are important to the SST evolution but otherwise the contributions from advection and entrainment terms appear negligible, which is expected given the weak horizontal and vertical temperature gradients in the region.

[29] In examining Figures 6 and 10–12, there are a number of other locations that exhibit responses to the MJO worth highlighting. These include the far eastern equatorial Pacific, the northwestern tropical Pacific, the subtropical regions in general, and the equatorial region around 170°E (Figure 15). The discussion of the latter will be taken up in section 4e. In regards to the far eastern equatorial Pacific, Figures 10 and 11 show a fair amount of SST variability in this region even though there is very little local forcing associated with the MJO. Examination of Figure 12 and an analogous figure of anomalous sea level (not shown) shows that the sea level variations (±5 cm) and zonal current variations in phase. This indicates that in addition to the enhanced TIW activity and the associated SST variability it induces, a large part of the anomalous SST variability occurring in the eastern Pacific is remotely forced via equatorial Kelvin waves. While this region of variability is geographically much more limited than the variability occurring to the west, it has about the same

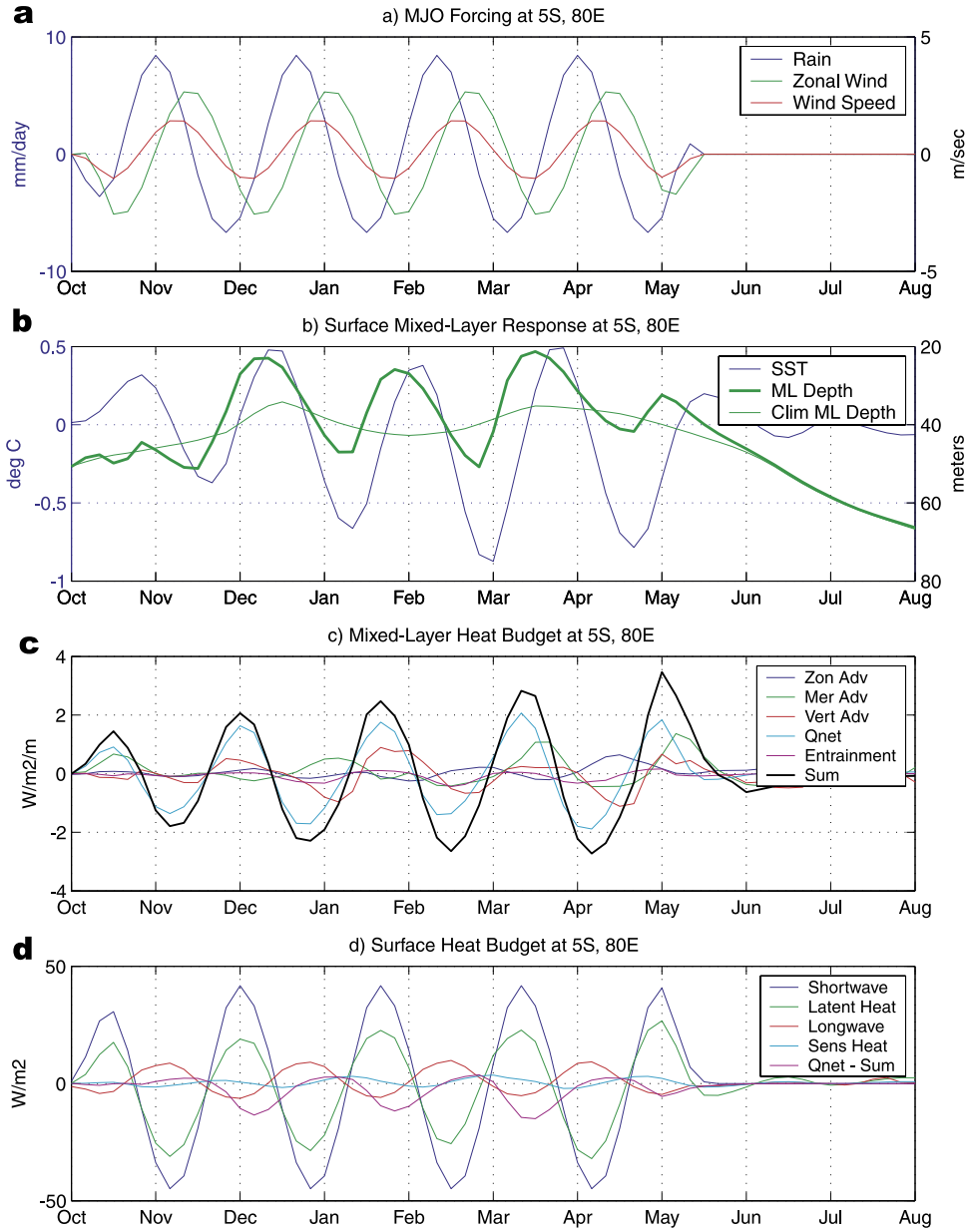

Figure 13. Time series averaged over a 1° × 1° box centered at 5°S, 80°E of (a) anomalous (i.e., composite) MJO forcing in terms of surface zonal wind (green), wind speed (red), and precipitation (blue). (b) Ocean model response in terms of anomalous SST (blue), total mixed layer depth (thick green) for case using MJO forcing, and climatological total mixed layer depth (thin green). (c) Anomalous values of mixed layer heat budget in terms of zonal (blue), meridional (green) and vertical (red) advection, net surface heat flux which accounts for solar penetration through the bottom of the mixed layer (aqua), entrainment (purple), and the sum of the above terms (black). (d) Anomalous values of surface heat budget in terms of net surface shortwave (blue) and longwave (red) radiation, latent (green) and sensible (aqua) heat flux, and the difference between the actual net surface heat flux that impacted the mixed layer and the sum of the above four terms (purple). This latter quantity is simply the shortwave energy that passed through the bottom of the mixed layer. In the above description, "anomalous" is taken to be the difference between the climatological simulation and the simulation forced with composite MJO conditions.

magnitude and has a systematic behavior relative to the forcing. In fact this behavior appears to be somewhat consistent with the sort of variability documented from observations by *Zhang* [2001, cf. *Harrison and Giese*, 1988; *Giese and Harrison*, 1991; *Vecchi and Harrison*, 2000; *McPhaden*, 2002].

[30] Details of the atmospheric forcing and near-surface ocean response associated with the far eastern Pacific region

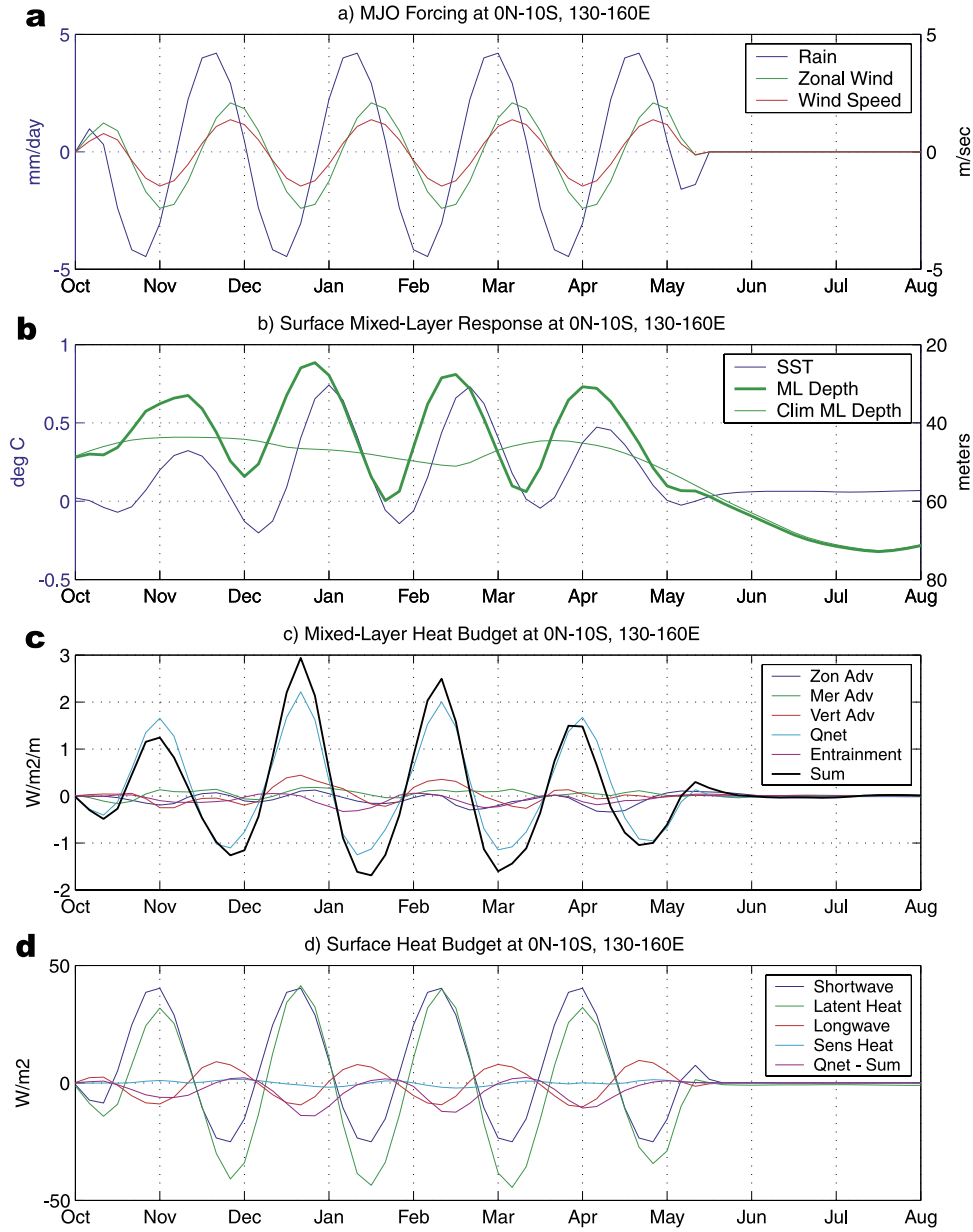

Figure 14. Same as Figure 13, except averaged over the domain 0–10°S and 130°–160°E.

discussed above are shown in Figure 16. Evident is the time lagged response between the zonal current and the applied forcing. Specifically, it can be seen that the oscillations in zonal current do not start until December, nearly two months after the imposed forcing begins in the basin, and extend through July, nearly two months after the forcing ends. Thus the in-phase relationship between the (small) local perturbations in zonal wind and the zonal current are somewhat circumstantial, the primary response is driven by wind forcing in the west. On the basis of the differences in the character of the positive zonal current anomalies in January, March, and April/May versus that in June/July, it is evident that the local wind does influence the response. The latter anomaly might be considered a free (Kelvin) wave while the former are waves influenced by local wind forcing. SST variations are on the order of 0.5°C and there are no systematic MLD variations, at least at the spatial scale of the domain being averaged. These SST variations are primarily driven by meridional advection, with contributions from net heat flux, zonal and vertical advection all being smaller but in phase with each other and leading the meridional heat flux by about a quarter cycle. This suggests that as a positive (negative) zonal current/sea level perturbation approaches, the initial warming (cooling) is produced by surface heat flux, changes in zonal advection as well as vertical advection. Still to be determined is whether the zonal (vertical) advection perturbations are dominated by perturbations in SST (vertical temperature gradient) or zonal current (vertical velocity). Once these three processes act to warm/cool the equatorial region, the meridional advection (determined primarily to be from $v'\frac{d\overline{T}}{dy}$) acts to spread this warming/cooling throughout the near-equatorial domain.

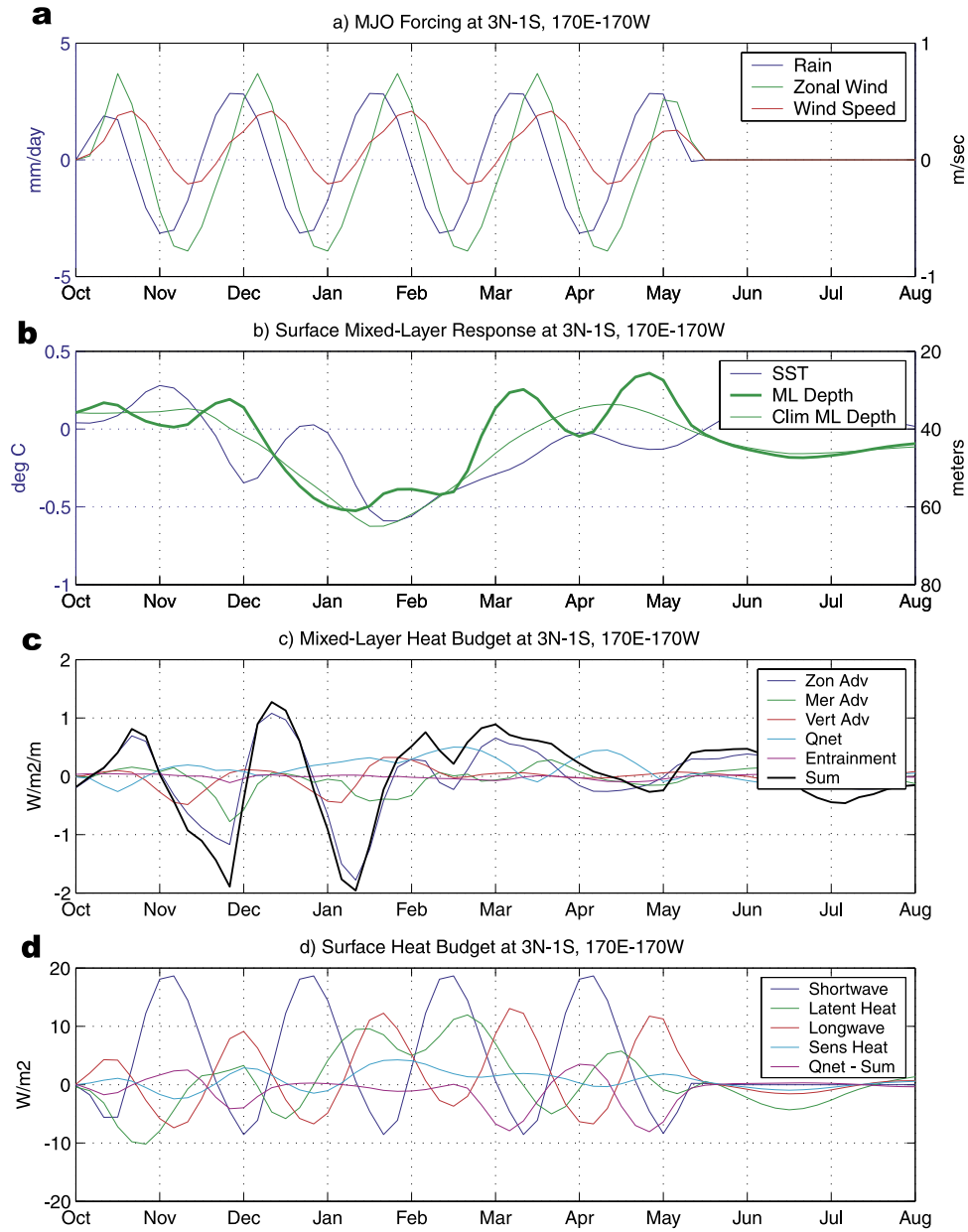

Figure 15. Same as Figure 13, except averaged over the domain 3°N–1°S and 170°E–170°W.

This process is somewhat consistent with the hypotheses given by *Zhang* [2001] and *McPhaden* [2002] although the details were less forthcoming in these studies given the limitations of the data (e.g., meridional advection could not be adequately determined). A highly relevant question concerns what mechanism is responsible for generating the anomalous meridional temperature advection (namely the v'). While it is worth noting that the local zonal wind forcing appears to be in a position to drive at least part of the anomalous meridional advection, an additional simulation performed with wind stress anomalies set to zero east of 140°W reduced the amplitude of the anomalous meridional advection by only 30–40%. This implies that other dynamical processes are at work to produce the anomalous meridional advection discussed above. The results of a more focused and conclusive examination of the above issues, that combines the model and observational analysis in a more synergistic fashion, will be reported in a future study.

[31] A region of weak SST variability occurs under the subtropical (15°–20°N) Asian jet around 140°E (Figures 10 and 11) that occurs in conjunction with modest cloud/shortwave and wind forcing. Plots such as those shown in Figure 13 for this location (not shown) illustrate that the SST variability is almost exclusively derived from surface heat flux forcing. Latent, shortwave and sensible heat flux are all in phase and act constructively to warm and cool the mixed layer with magnitudes of about ±30, 15 and 5 Wm^{-2}, respectively, and net longwave acting destructively with a magnitude of about ±10 Wm^{-2}. For this location, the SST response is very sensitive to the climatological MLD. For example, the first (~November) and last (~April) event occur when the climatological mixed layer depth are around

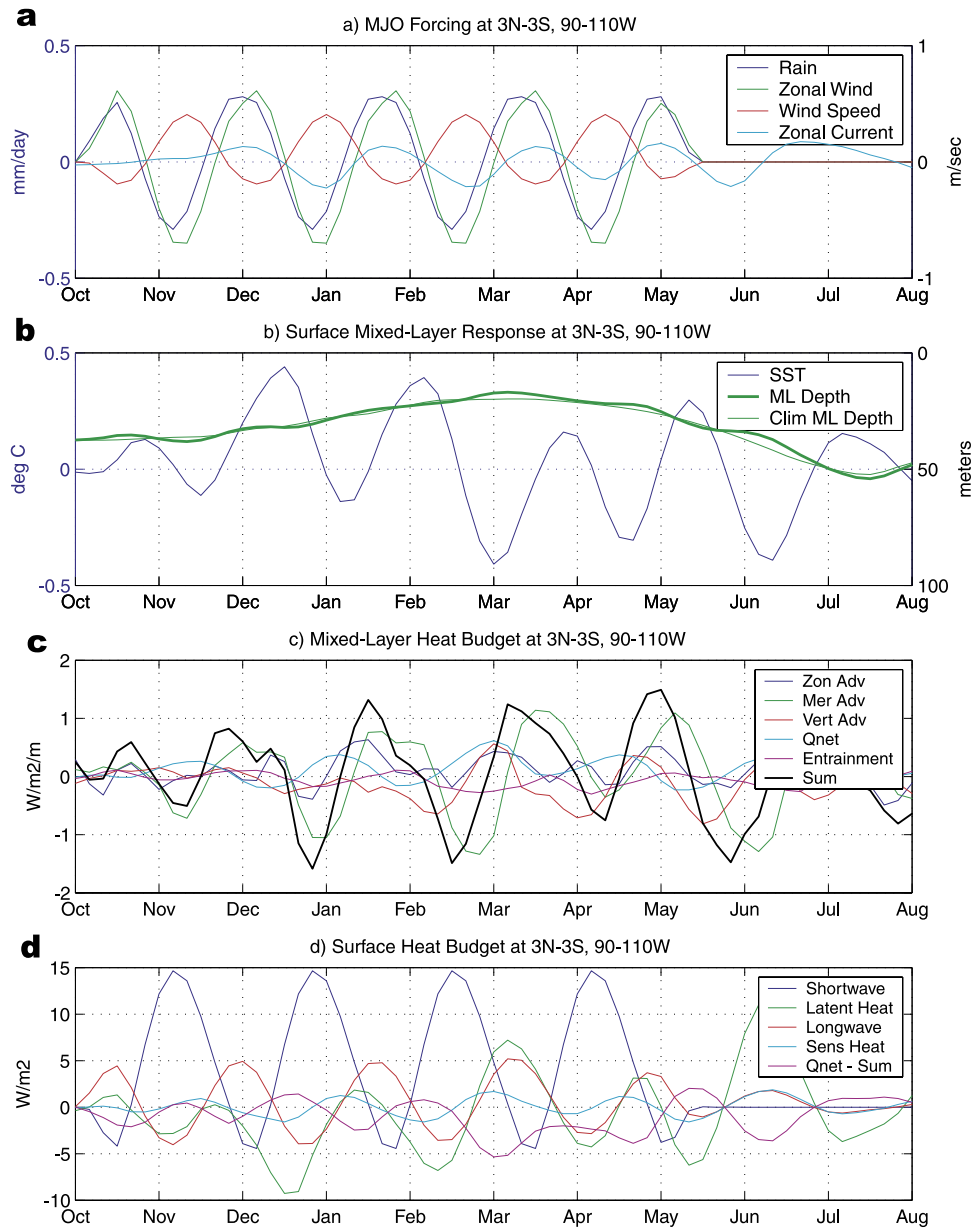

Figure 16. Same as Figure 13, except averaged over the domain 3°N–3°S and 90°W–110°W and including the zonal current in the top panel.

60 m while the intervening two occur when the MLD is 100 m (the model's maximum MLD). Under the shallower mixed layer conditions, the SST variations are on the order of 0.3°C while under the deep conditions the SST variations are considerably smaller. It should be noted that during the summer months (~May–October), the character of the intraseasonal forcing changes [e.g., *Wang and Rui*, 1990] and under these climatological conditions, the local forcing associated with the MJO is considerable. The ocean response under these conditions will be explored under a similar framework in a separate study.

[32] Finally a comment is in order regarding the model's subtropical response to the imposed MJO forcing is in order given that in these regions there is considerable MLD variability (Figures 10 and 11). Figure 6 shows that concomitant with this MLD variability is a fair amount of wind (stress) variability as well as modest amounts of cloud and shortwave variability. While these regions do not exhibit much SST variability, it is instructive to briefly illustrate the relevant processes. Plots such as Figure 13 for these subtropical regions (not shown), along with other analysis, show that these regions are typically characterized by a very deep climatological mixed layer and relatively less stratification – given the cooler surface waters. The intraseasonal wind forcing is relatively strong and induces intraseasonal fluctuations in MLD on the order of 30 m. For example, in the region around 20°N and 165°W, the MLD is typically 100 m. Under the low wind speed phase of the MJO forcing, the MLD decreases to 70 m. This MLD change is rather large relative to that occurring in the deep

tropics (e.g., Figures 11 and 12) although relatively small when considering the climatological value. Moreover, because the net surface heat flux anomalies are still rather small, about 20 Wm^{-2}, and the total MLD is large, the SST fluctuations remain very small ($\sim$0.1°C).

4.3. Sea Level and Transports

[33] As mentioned earlier, relatively large sea level variations occur on the eastern side of both ocean basins (Figure 10). This, in conjunction with the zonal current composite (Figure 12) and sea level composite (not shown) indicate that this activity stems from equatorial Kelvin waves. In the case of the Indian Ocean for example, these waves produce sea level variations on the order of 5–10 cm and travel from the central part of the basin well into the Bay of Bengal and down the southern coast of Java and into the Indonesian seas. While the Kelvin waves in both basins appear to be derived from MJO wind forcing, it is worth noting that the zonal scale of the waves in the Pacific Ocean is on the order of 4000 km while the zonal scale in the Indian Ocean is only about 1000 km. Associated with this sea level and current variability are variations in basin-wide transports. In this discussion, only the Indonesian Throughflow (ITF) and the cross-equatorial Indian Ocean transports will be highlighted. Figure 17 shows the model heat (and mass, see caption) transports associated with the applied canonical MJO forcing. In Figures 17a, 17b, 17e, and 17f, the results are put into the context of the climatology, while Figures 17c, 17d, 17g, and 17h simply show the anomalies. Rather remarkable in the case of the ITF (upper set of four plots) is that the magnitude of the intraseasonal variability ($\pm\sim$1 PW) forced by the MJO is at least as large as the annual cycle, and equally as large as estimates of interannual variability in the ITF [*Murtugudde et al.*, 1998]. However, since the timescale is relatively short, the effects of this variability on the heat and mass budgets of the Indian Ocean basin as a whole may not be important although they appear to play a role in the evolution of the Indian Ocean Dipole/Zonal Mode (IOZM) [*Annamalai et al.*, 2002]. Further investigation is required to see if the ocean integrates these heat transports into secular trends in the Indian Ocean [*Webster et al.*, 1999]. Since the SST trends may affect the MJO activities [*Slingo et al.*, 1999; *Zveryaev*, 2002], it would be of interest to determine if there are any feedbacks from the MJOs to the secular trends in SST. However, the adjustment to the changes in the transports and the remotely forced waves appears to be local off the coast of Java [*Sprintall et al.*, 2000; *Potemra et al.*, 2002].

[34] In contrast to the ITF, the relative sizes of the climatological and anomalous cross-equatorial Indian Ocean transport are just the opposite. The annual cycle of the north-south heat transport, which has been hypothesized to play an important role in the coupled ocean-atmosphere regulating system of the Asian monsoon [*Loschnigg and Webster*, 2000], has an amplitude of about ±2 PW. On the other hand, the range of the intraseasonal variations is only about ±0.5 PW. These variations are rather weak relative to the ITF because of the orientation of the wind variability (i.e., mostly zonal), the anomalies do not penetrate as deep ($\sim$<100 m), and there is a baroclinic nature that leaves only relatively small residual values. In any case, it would be of some interest if the net effect of a given MJO event produced a net nonzero transport response in either type of transport described above. Such a condition could arise because of stratification changes and modest wind asymmetries associated with the MJO. The results discussed above indicate that very little such rectification appears to occur. Additional considerations of the low-frequency rectification of the model's MJO response will be discussed below.

4.4. Rectification to Low Frequencies

[35] Apart from the intraseasonal fluctuations shown in Figure 13–14, there also appears to be a rectification of the intraseasonal model response onto lower frequencies. For example, in both Figures 13 and 14 the mean MLD over the period of the active MJO forcing is less than for the model's climatological MLD. Similar low-frequency variations occur in the SST. These low-frequency characteristics are more evident in the near-equatorial time-longitude diagrams shown Figure 18a as well as the maps of the mean anomalous response shown in Figure 19. The latter illustrates that the application of the control case MJO forcing to the ocean model leads to a slight warming ($\sim$0.3 C) in the region of the maritime continent during the period of active MJO forcing. Concomitant with this low-frequency warming is a mixed layer shoaling of about 5 m. In addition, the equatorial western Pacific exhibits a mean westward current bias of about 10 cm s^{-1} and the Indian Ocean exhibits a small amount of MLD shoaling ($\sim$4 m) with a modest change in the large-scale, east-west SST gradient (discussed further below).

[36] The only other study to examine the low-frequency/mean ocean response to applied MJO forcing is that of *Kessler and Kleeman* [2000] (hereinafter referred to as KK). Their study employed a Tropical Pacific-only version of the Gent-Cane ocean model to study the low-frequency rectification of the MJO (especially to the interannual timescale via MJO influences on ENSO). On the basis of idealized, analytic MJO forcing (i.e., eastward propagating, sinusoidal wind stress anomalies) that did not include buoyancy perturbations associated with rainfall or solar radiation, they found that the MJO forcing leads to a mean SST cooling ($\sim$0.4°C) and eastward zonal current bias ($\sim$20 cm s^{-1}) in the western Pacific Ocean. While an equatorial cooling is observed for the control case forcing presented here, it is considerably weaker, and the sign of the rectified current in the present case is negative while theirs was positive. The differences in these two results, particularly that associated with SST, appears to result in part from the neglect of the buoyancy forcing terms in the KK study, especially shortwave, as well as to the application of an absolute low wind speed threshold (>= 4 m s^{-1}). Another difference is that the KK simulations were done with half the vertical resolution. This would greatly affect the stratification below the mixed layer and exaggerate the surface cooling because of entrainment. Also, it would enhance mixed layer deepening due to penetrative heat fluxes [*Murtugudde et al.*, 2002]. Figures 18b and 19b show our model results when the composite MJO perturbations associated with rainfall and shortwave were excluded from the MJO forcing. Apparent is an increased SST cooling and reduction in the MLD shoaling over the Indo-Pacific region relative to the control case MJO forcing. A similar case that neglected only the shortwave perturbations showed results similar to this case,

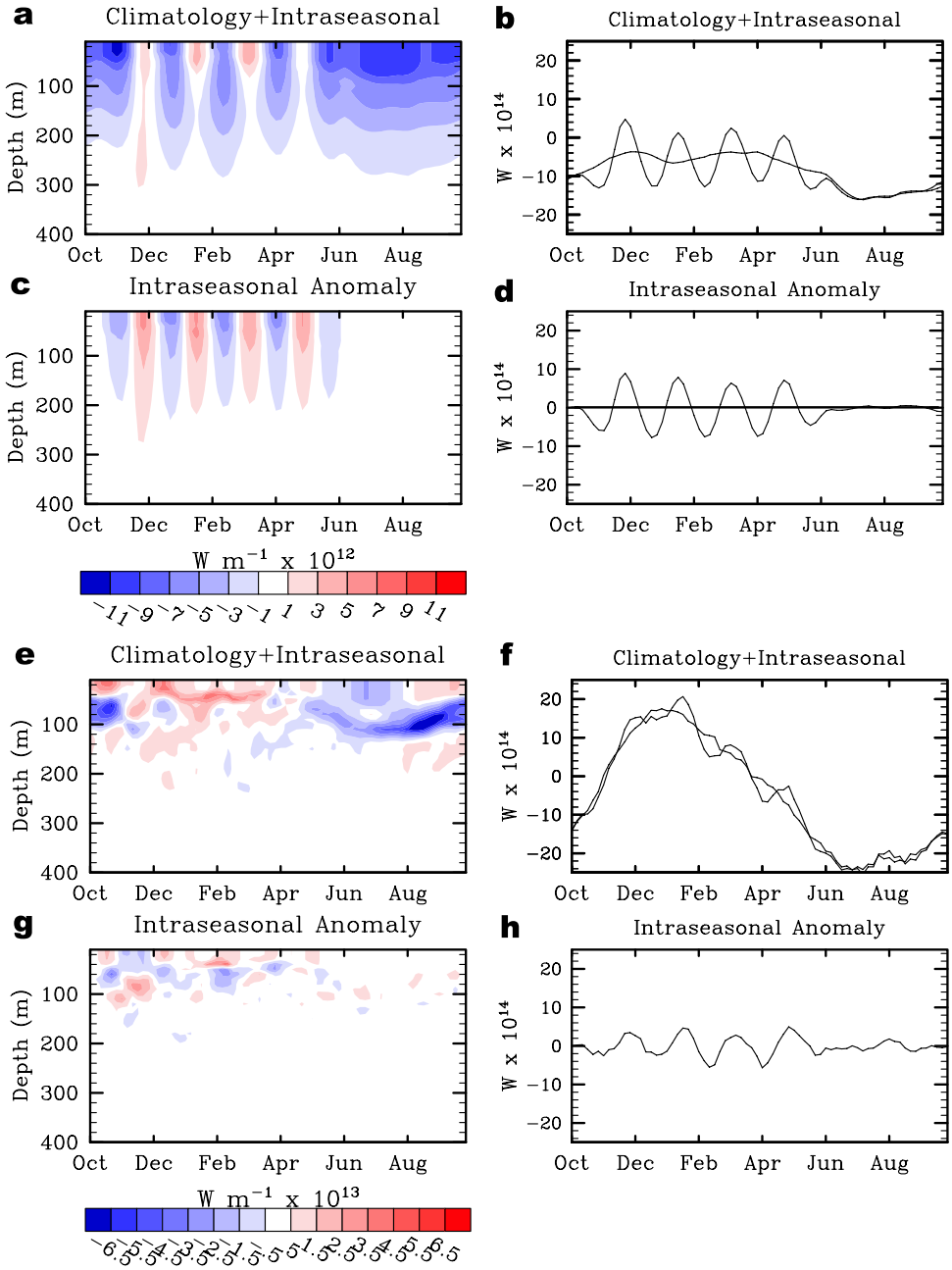

Figure 17. (a) Total zonal heat transport across 114°E as a function of time and depth for the simulation using MJO forcing. (b) Depth integrated (z < 400 m) heat transport across 114°E as a function of time. The smooth line is the climatological value. (c) and (d) Same as Figures 17a and 17b, except showing the differences between the case with and without (i.e., climatology) MJO forcing. (e)–(h) Same as Figures 17a–17d except for cross-equatorial transport in the Indian Ocean. Note the scale change between the top and bottom sets of contour plots. Mass transport plots (not shown) look very similar except that the units and scales for the color bars are $m^2\ s^{-1} \times 10^4(10^5)$ for the top (bottom) set and units and scales for the line plots are $m^3\ s^{-1} \times 10^6$.

indicating that most of the difference observed between the Figures 18a–19a and 18b–19b is attributed to the absence of anomalous shortwave forcing.

[37] Figures 18c and 19c show our model results from simulations without the surface buoyancy perturbations, and when an absolute critical wind speed threshold was employed (>= 4 m s^{-1}). This absolute threshold inhibits the reduction of the sensible and latent heat fluxes that normally act to enhance the warming during the low wind speed phases of the oscillation [e.g., *Anderson et al.*, 1996; *Weller and Anderson*, 1996; *Jones et al.*, 1998; *Shinoda et al.*, 1998]. In this case, the SST barely warms in the suppressed phase of the MJO. This is due not only to the direct effect from the excluded shortwave anomalies on

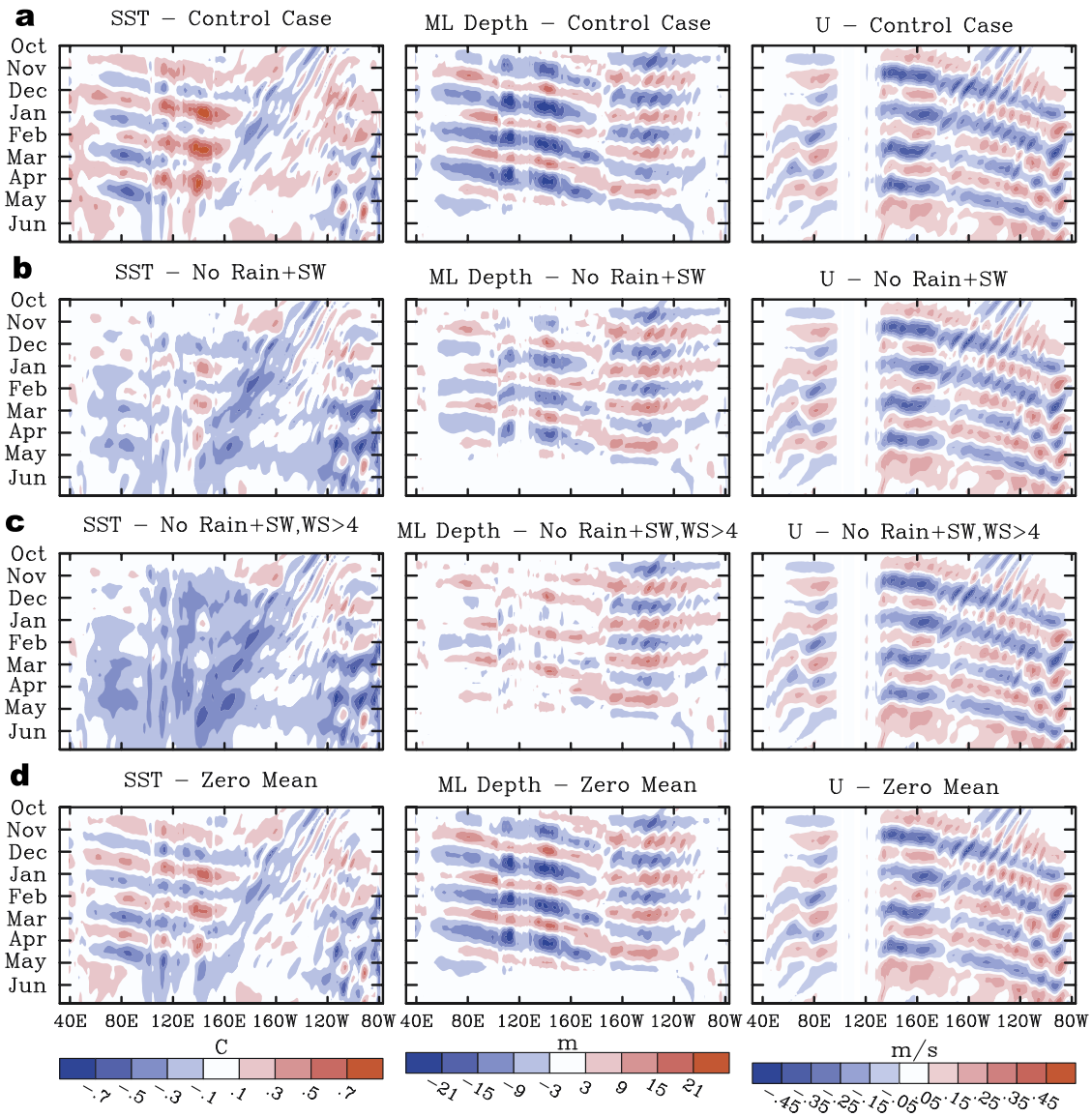

Figure 18. Time-latitude diagrams of anomalous ocean response in terms of (left) SST, (middle) mixed layer depth, and (right) surface zonal current associated with (a) MJO forcing for the control case, (b) no anomalous rain or shortwave forcing, (c) no anomalous rain or shortwave forcing and with a lower limit wind speed threshold of 4 m s^{-1}, and (d) as in the control case (Figure 18a), except with the residual means of the MJO cyclic forcing structure removed (see section 3b). The latitude band used for the SST and mixed-layer depth (zonal current) is 3°N–7°S (3°N–3°S).

the mixed layer but also because application of a wind speed minimum leads to an increased mixed layer depth over the whole MJO cycle relative to the control case MJO forcing; the latter of which inhibits SST warming. Figure 19 shows that the low-frequency SST warming signatures and shallower MLDs exhibited around the Maritime continent in the control case are nearly absent in this case, and in fact are replaced with net SST cooling and MLD deepening. In fact this cooling signature, which is most pronounced around the Maritime continent, extends over a broad region of the Tropical Indo-Pacific Ocean. One can surmise from Figures 13 and 14 that if shortwave anomalies were neglected from the MJO forcing, and the MLD was not allowed to shoal because of the imposition of a wind speed threshold, the SST warming that occurs during the suppressed phase of the MJO would be greatly curtailed. These results indicate that the shortwave and wind anomalies can act in conjunction to produce a rectified warming. This occurs because high shortwave occurs in conjunction with low wind forcing periods (i.e., suppressed phase of the MJO) and both of these act to shallow/stabilize the mixed layer leading to a greater heating rate from the positive (negative) shortwave (wind) anomalies. In contrast, during the convective/high wind forcing phase, the mixed layer deepens and the negative (positive) shortwave (wind) anomalies act on a deeper mixed layer which reduces the magnitude of the heating rate (i.e., actually cooling in this case) relative to the suppressed phase of the MJO.

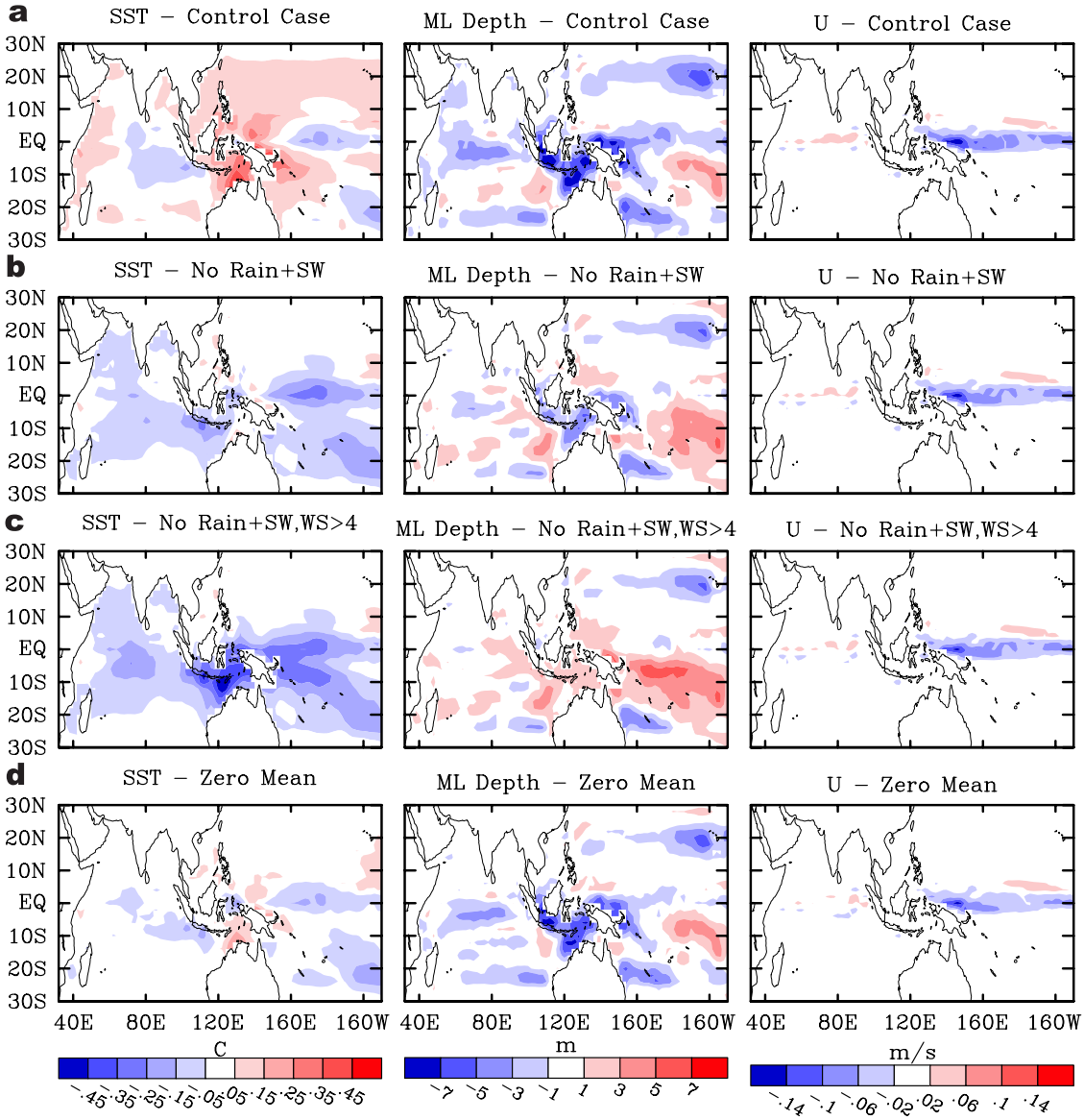

Figure 19. Time mean maps of anomalous ocean response in terms of (left) SST, (middle) mixed layer depth, and (right) surface zonal current associated with (a) MJO forcing for the control case, (b) no anomalous rain or shortwave forcing, (c) no anomalous rain or shortwave forcing and with a lower limit wind speed threshold of 4 m s^{-1}, and (d) as in the control case (Figure 19a), except with the residual means of the MJO cyclic forcing structure removed (see section 3b). Time averages were taken over the four complete MJO cycles, i.e., pentads 4–43 (see section 3 and Figure 4).

[38] The SST results from the 3rd case described above appear to be very consistent with the results shown by *Kessler and Kleeman* [2000, Figure 3]. They suggested three mechanisms were responsible for producing the rectified signals found in their experiments. The first mechanism was associated with the wind threshold and its effect on latent (and sensible) heat flux. The second mechanism is associated with the nonlinear response of the equatorial zonal current to oscillating zonal winds. This mechanism (see their discussion) [*Robinson*, 1966; *Gill*, 1975] accounts for their net eastward zonal current on the equator and the slight net SST warming found to the east of their strong SST cooling region. The third mechanism is associated with the correlation between the anomalous upwelling and vertical temperature gradients associated with the MJO forcing. Summarizing their discussion in regards to the latter mechanism, under easterly wind forcing, and thus upwelling, the vertical temperature gradient is stronger and thus a net cooling results over the cycle. In general, the first and third (second) mechanism account for the bulk of the SST (zonal current) rectification found in their experiments. As demonstrated in their study and above, the first mechanism clearly plays an influential role on the SST. The analysis above demonstrates the additional impact it has on MLD and in turn the MLD's impact on the SST. In light of the frequently sampled (i.e., 15-minute) record obtained for a

number of MJO events during TOGA-COARE [e.g., *Weller and Anderson*, 1996, Figure 9], it isn't obvious that such a threshold is appropriate for the suppressed wind phase of the MJO since there doesn't appear to be any unsampled gustiness that would need to be accounted for within the imposed forcing. In regards to the third mechanism, it is undoubtedly acting in the present simulations as well. In fact, since the surface warming in the easterly wind phase is greater in the present study, its effects would be expected to be even larger. This might account for the fact that even though the rectified signal over most of the Indo-Pacific Ocean is considerably warmer in Figure 19a relative to Figure 19c, the change is somewhat smaller over the equatorial western Pacific where this mechanism would be expected to be acting.

[39] While the above results and discussion help to explain the differences in the rectified SST signal between KK and those presented here, they do not explain the difference in the rectified zonal current signal. Even the MJO forcing case presented here that tried to mimic that of KK (i.e., Figures 18c and 19c) still shows a net westward zonal current while their rectified current was eastward in this region. The equatorially trapped nature of the signal, as well as a simulation performed in which wind stress perturbations were neglected from the MJO forcing (not shown), indicate that this feature derives almost solely from interactions with the wind stress forcing. It is reasonable to presume that the second rectifying mechanism discussed above is acting in the present model and thus the model should have a tendency for a rectified eastward current. However, an additional mechanism is acting in the present experiments, one that is likely to be less pronounced in those of KK. As illustrated in Figure 18 (middle), MLD changes are considerable in the control case MJO forcing. In fact there is about a 20 m difference in MLD between easterly and westerly zonal wind phases (this is against a background MLD of ~40 m; see also Figure 13). Since the MLD is less during the easterly phase, a somewhat similar momentum input (Figure 6) between the two phases results in a stronger westward current during the easterly phase than the eastward current during the westerly phase. In fact, it would appear that this effect is significant enough to overcome the second mechanism discussed above.

[40] As a final remark regarding MJO-induced rectification in the ocean, it is important to clarify the degree to which the rectification exhibited in the control case (Figures 18a and 19a) stems from actual ocean rectification processes versus a rectified signal in the MJO forcing itself. As discussed in section 3b, the method used for compositing did not require the forcing associated with the "anomalous" MJO cycle to have zero mean (albeit the "residual" means were small). Rather, the intention was to simply try and capture an accurate depiction of an MJO event, with specific effort made to limit biasing of the forcing that might arise from interannual variability (i.e., via band passing). To determine the influence that these residual means have on the rectified signal, a simulation was carried out in which the residual means were removed from the composite MJO forcing components (i.e., solar, winds, clouds, and rain). The results of this experiment are shown in Figures 18d and 19d. Note that in general, the same qualitative behavior, albeit with weaker amplitude, occurs for this case as for the control case. Thus, at least some part of the rectified behavior exhibited in the control case arises solely because of the nonlinear response of the ocean model to the imposed forcing and is not derived from any rectified/mean effect in the MJO forcing itself.

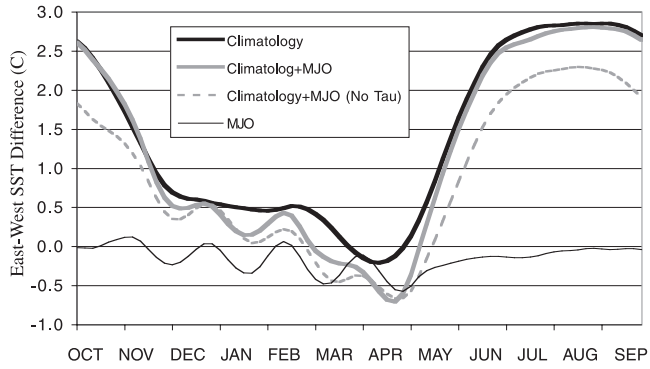

Figure 20. SST difference across the tropical Indian Ocean for the model climatology (thick black), the control case with MJO forcing (thick gray), the MJO forcing case with no wind stress (gray dashed), and the difference between the climatology and control case with MJO forcing (thin black). The SST in the eastern (western) Indian Ocean was computed by averaging the SST over the region 0–10°S, 80°–100°E (0–10°S, 40°–60°E).

[41] Another feature worth highlighting is that independent of the forcing scenario discussed above, the cool phase of the SST in the central Indian Ocean has an evolving nature in which each successive event has a slightly larger negative value. This seems to be related at least in part to the fact that the curl of the composite MJO wind anomalies is 50% larger during the negative phase than for the positive phase (not shown). Note that the negative wind curl phase occurs in conjunction and just after the convective phase of the MJO. This is important because the climatological thermocline depth tends to be relatively shallow in the central Indian Ocean [*Murtugudde and Busalacchi*, 1999], particularly just south of the equator. Thus the negative wind stress curl anomaly phase has the potential for contributing more to the SST cooling than the positive wind stress curl anomaly phase. This aspect of the results is presently being examined in more detail using additional observational data (e.g., TOPEX, TMI) to determine the extent to which this behavior is exhibited in the observations. This, as well as a more focused model analysis will be used to determine the mechanisms responsible for the temperature fluctuations in this region, including their evolving nature.

[42] The last aspect regarding low-frequency rectification concerns the influence the MJO may have on the possible development of the IOZM [e.g., *Murtugudde and Busalacchi*, 1999; *Saji et al.*, 1999; *Webster et al.*, 1999]. The SST panels in Figure 18 show that the SST can be slightly out of phase between the eastern and western Indian Ocean. Given that an analog to the Bjerkness hypothesis has been suggested to possibly play a role in the development of the IOZM, it is worth considering how the MJO might influence the SST gradient across the Indian Ocean. Figure 20 shows time series of the SST difference across

the Indian Ocean basin for the model climatology (thick black) and the case with MJO forcing (thick gray). During late boreal winter, the IOZM is most prone to grow because of the weakened and nearly reversed east-west SST gradient. When MJO forcing is imposed on top of the climatological forcing, the impact on the SST gradient can be quite substantial in relative terms (~50%) given its relatively small magnitude during the time of the year when MJO is most active. A simulation without the wind stress anomalies associated with the MJO forcing (dashed gray) indicates that most of the SST gradient change is accomplished solely by the surface heat flux perturbations. *Annamalai et al.* [2002] hypothesize that the remotely forced precipitation anomalies during boreal spring months off Java initiate the anomalous upwelling winds which lead to the initiation of the SST cooling and the Bjerkness feedbacks. Our results indicate that MJO-related surface heat fluxes may be preconditioning the SST gradient at the same time and the two processes may be acting in concert to influence the development/evolution of the IOZM. More detailed modeling and observational analysis is being carried out to focus on this interplay and the results will be reported elsewhere.

4.5. Three-Dimensional Processes Versus Slab Ocean

[43] As mentioned in the Introduction, the study by *Waliser et al.* [1999] showed that the coupling of a slab mixed layer ocean to an atmospheric GCM had a positive influence on the model's representation of the MJO. This section will briefly explore the fidelity of such a slab ocean for representing the SST variability induced by MJO forcing, this procedure also serves to illustrate where ocean dynamics play an important role. In the above study, net surface heat flux anomalies were applied to a 50 m slab ocean to obtain SST anomalies that were then added to the otherwise fixed (climatological) SST. To mimic that approach, the surface net heat flux anomalies from the control case are used here to force a slab mixed layer to derive the associated SST anomalies. To first examine the dependence of the response on the MLD, the forcing was applied to slabs of various depths from 10 to 90 m. On the basis of a comparison of the size of the induced SST variability to the size of the variability obtained in the GCM (i.e., Figure 10) and from a computation of the RMS difference in SST anomalies from the two models, it was found that a slab depth of about 30–50 m gave the most similar results, at least for Indo-Pacific warm pool region. This is not surprising given the model's climatological MLD is about 40 m in this region (see Figures 13 and 14). Figure 21 shows the results from this comparison for the 40 m slab ocean, along with a time-longitude diagram of the SST. Overall, the evolution of the SST along the path of the MJO and the region of significant MJO-induced variability are both quite similar to that shown in Figures 18 and 10, respectively. In each case the magnitude for the slab mixed layer is less than for the OGCM because of the systematic MLD shoaling (up to 20 m) that occurs in the OGCM during warm SST periods. The RMS difference map shows that the typical SST differences between the two models is on the order of the variability itself. The much larger errors that occur in the eastern Pacific tend to be associated with the lack of dynamic variability (e.g., TIW) in the slab model and the lack of remotely forced thermocline/mixed layer interactions.

[44] The correlation map shows that most of the SST variability in the OGCM is in phase with that of the slab mixed layer. This simply implies that surface heat flux tends to be the dominant process in most cases and thus determines the phase of the variability in the OGCM as well as of course the slab ocean. However, of interest are the areas of negative correlation since these would indicate areas where ocean dynamics must be determining the phase of the SST variability. Here, we will focus only on the area at and just north of the equator in the western Pacific Ocean. The other areas of negative correlation occur in regions where the net surface heat flux forcing and SST response are rather weak. However, the area in the western Pacific Ocean is rather unexpected and to some extent should be viewed with caution. Figure 11 shows an alternative representation of this feature whereby the SST in this region tends to be out of phase with the SST to the south and to the east around the maritime continent but tends to be in phase with the SST in the Indian Ocean. Figure 15 shows the temporal evolution of a number of forcing and response indicators for this region. The most striking feature is that for the first two to three MJO events, the zonal advection (driven by the zonal wind) dominates the mixed layer heat budget response and this is out of phase with the weaker net surface heat flux values; hence the correlation seen above. Note that the strong signal observed in zonal advection for just the first two to three events stems mostly from the fact that the magnitude of the background zonal temperature gradient in this region is a maximum during the November through February time frame and weakens to about half this maximum value after February and for the remaining of the anomalous MJO forcing period.

[45] On the basis of the model SST bias (Figure 1) which indicates a maximum error in the east-west gradient around the dateline, we suspect the OGCM might be over emphasizing the contribution from zonal advection in this region. However, we would also like to point out that nearly all of the studies that have examined this issue have either focused on the region south of the equator [*Hendon and Glick*, 1997; *Shinoda et al.*, 1998, 1999], analyzed an area east of this region where the zonal gradient is weak [*Zhang*, 1996; *Lau and Sui*, 1997], or considered a band equally weighted north and south of the equator [*Woolnough et al.*, 2000] which might obscure different behavior between the region just north and south of the equator in this region. The spatial diagrams of correlation between observed SST and other MJO-related quantities by *Hendon and Glick* [1997] and *Jones et al.* [1998] do show that the simple relationship between surface heat flux and SST variability tends to be stronger (weaker/nonexistent) south (north) of the equator. However, no observational study has sought to determine to what extent this characteristic is robust or to distinguish the reasons for this north/south difference. The OGCM experiments presented here suggest the possibility that apart from what might simply be weaker surface heat flux forcing in this region, a more ambiguous relationship could very well be occurring because of the elevated importance of three-dimensional ocean processes. This issue deserves further research, particularly in light of the possible role that SST coupling may play in the development and maintenance of

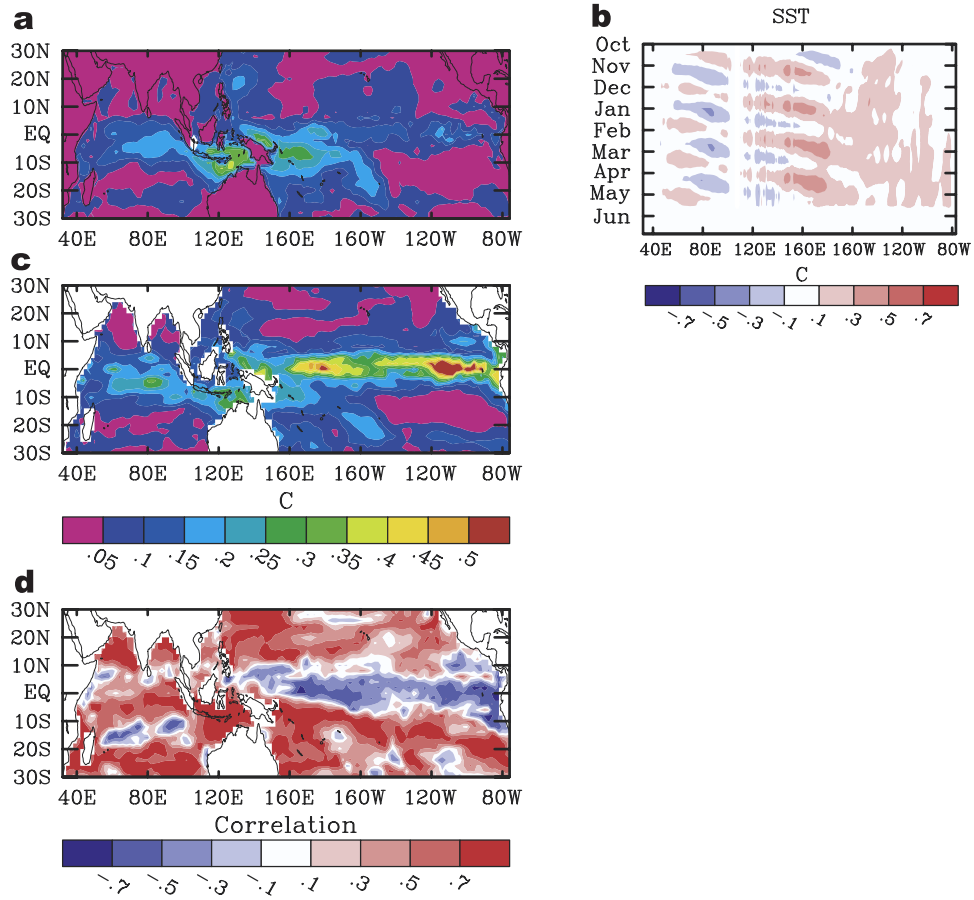

Figure 21. (a) Anomalous SST variability from a 40 m slab mixed layer forced with the anomalous net heat flux from the GCM model simulation with control case MJO forcing (see section 4e); analogous to Figure 10 (top left). (b) Same as Figure 18 (left), except as derived from a 40 m slab mixed layer forced with the anomalous net heat flux from the model simulation with control case MJO forcing. (c) and (d) Root mean square difference and correlation between the slab mixed layer model SST described above and the OGCM simulated SST with control case MJO forcing.

the MJO as it propagates from the Maritime continent to the central Pacific Ocean/SPCZ region.

5. Summary

[46] The objective of this study was to examine the basin-wide response of the Indo-Pacific Oceans to atmospheric forcing associated with the MJO. The purpose was to obtain a comprehensive view of the ocean variability that might be directly attributed to the MJO and to examine the mechanisms underlying this variability. In doing so, our intention was to broaden the perspective offered by previous studies whose findings were necessarily limited because of observational constraints [e.g., *Cronin and McPhaden*, 1997; *Ralph et al.*, 1997; *Feng et al.*, 2000; *Zhang and McPhaden*, 2000; *Zhang*, 2001], simplified model physics [e.g., *Shinoda and Hendon*, 1998] and/or regional dependencies [e.g., *Zhang and Rothstein*, 1998; *Shinoda and Hendon*, 2001]. Because of the relative abundance of atmospheric (forcing) data and the relative paucity of ocean (response) data, an ocean GCM framework with imposed forcing was utilized. Significant care was taken to develop canonical forms of MJO forcing from the available observations (Figures 2–6) and then to use them with an ocean GCM that demonstrates reasonable fidelity in representing the ocean response to MJO forcing (Figure 9) [see also *Shinoda and Hendon*, 2001]. The primary issues addressed in this study involved determining: 1) the general scope of tropical ocean variability that could be attributed to typical MJO forcing (e.g., regional dependence, strength of response, local versus remote), 2) the particular components of the forcing that were the most important; and 3) the relative contributions of the different physical mechanisms responsible for the ocean response. In this study the response was measured in terms of physical properties, such as circulation, temperature, mixed layer depth (MLD), salinity and sea level variations. In addition, a number of more specific issues were examined, such as the effect on basin-scale transports, remote effects via wave propagation, rectification of the intraseasonal timescale to lower frequencies, and the degree to which 3-D ocean physics are required to represent the ocean's temperature response.

[47] The results show that the imposed MJO forcing induces ocean variability that is both local to the region of intense convective activity (i.e., Indo-Pacific warm pool) as well as considerable variability outside this region

(Figures 10–12). The former consists of variations, measured in terms of standard deviation, that range up to about 0.5°C in SST, 15 m in MLD, 0.2 (0.1) m s^{-1} in surface zonal (meridional) current, 4 cm in sea level, and 0.08 psu in salinity. The salinity variations are rather small relative to the gradients in the basin-wide salinity field, however the variability in the other quantities is significant. While the nature of SST variability associated with the MJO has been documented in a number of studies, the variability of MLD and surface currents, and its implications, are associated with more uncertainty (see Introduction). The findings in this study, based on the OGCM as well as a slab mixed layer, suggest that in regions around the maritime continent and south of the equator in the western Pacific warm pool, the SST variations are driven to a large extent by the net surface heat flux variations (Figure 14). However, in regions close to and just north of the equator in the western Pacific warm pool (Figures 15 and 21) as well as in the near-equatorial Indian ocean (Figure 13), three-dimensional ocean advection processes play a nontrivial role, and can range up to 50% or more of the size of the net surface heat flux variations. Consistent with earlier studies and expectations, the main contributing forcing components are wind stress, wind speed via its effects on evaporation, and cloudiness via its effect on shortwave. Other components of the forcing, such as rainfall, cloud cover effects on longwave, and sensible heat flux in general, make much less contribution to the ocean variability. In terms of magnitude and phase, variations in shortwave and latent heat flux are considerable and tend to act in phase to heat/cool the SST, variations in longwave are modest but tend to be out of phase with the shortwave, and variations in sensible heat flux are negligible. In the Indo-Pacific warm pool areas discussed above, MLD variations were also found to be considerable (e.g., Figure 11) and important in determining the SST variability. For the most part, these variations contributed in a positive manner to the SST variations. For example, the MLD shoaling during the heating phase of the MJO induced additional SST heating that is not present under fixed MLD conditions (e.g., compare Figures 18 and 21). However, in some cases this shoaling became so significant (~20 m) in the context of the background MLD (~40 m) that nontrivial amounts of solar radiation penetrated through the bottom of the mixed layer [e.g., *Anderson et al.*, 1996].

[48] Apart from the Indo-Pacific warm pool areas discussed above, the ocean variability in a number of other regions that stemmed from MJO forcing was examined. For example, the remotely forced SST variability that develops in the eastern equatorial Pacific was found to be generally consistent with the observed variability documented by *Zhang* [2001], having broad longitudinal (~4000 km) and latitudinal (~500 km) extents and occurring in conjunction with the propagation/arrival of ocean Kelvin waves from the western Pacific (Figures 11, 12, and 16). While the TOGA/TAO array data analyzed by Zhang suggested that vertical entrainment is the primary mechanism for producing the observed SST variability, analysis of the model's heat budget suggests that advective processes, namely meridional advection, might play more significant roles. A separate, more focused, study is now underway to determine more specifically the processes responsible for generating this component of east Pacific SST variability. While the subtropical areas were largely devoid of MJO induced ocean variability, except for the SPCZ, a region of modest SST variability occurs just east of S.E. Asia/China (Figure 10) because of variations primarily in surface heat flux. The SST response in this region is highly dependent on the time of year the MJO occurs because of the significant climatological variations in the (model) MLD. During the boreal fall and spring (winter), when the climatological MLD is about 60 m (100 m), the SST variations are on the order of 0.3°C (0.1°C). In addition, a large fraction of the subtropics exhibits MLD variations as large as those occurring in the Indo-Pacific warm pool. In general however, these are associated with very minor variations in SST because of the much larger climatological MLD that occur in these regions (i.e., ~100 m). The modest MJO-induced wind stress and heat flux forcing combines with the weaker stratification that is typical of these regions to produce the intraseasonal MLD variations on the order of 30 m which is large relative to the variations exhibited in the Indo-Pacific warm pool regions but small in the context of the climatological values in the subtropics.

[49] In conjunction with MJO wind stress forcing are remotely forced sea level variations (~5–10 cm), via Kelvin waves, on the equator and the eastern sides of the Indian and Pacific Ocean basins (Figure 10). In conjunction with these sea level variations are variations in basin-wide transports (Figure 17). For example, variations the Indonesian Throughflow (ITF) brought about by MJO wind stress forcing are of the same order as the magnitude of the seasonal cycle of ITF transport (~1 PW; 10 Sv). While the relatively short timescale associated with the MJO, and somewhat cyclic nature, may keep these variations from having large net impacts on the heat/mass budgets of the Indian Ocean as a whole, recent evidence suggests that these MJO-induced ITF variations may play a role in the evolution of the Indian Ocean Zonal Mode (IOZM) [*Annamalai et al.*, 2002]. In contrast, the variations associated with the climatological cross-equatorial flow in the Indian Ocean basin are considerably larger (~4 PW) than those associated with MJO forcing (~<1 PW).

[50] Considerations were made to address whether and how the intraseasonal timescale of the MJO forcing might lead to longer timescales of variability in the ocean (Figures 18 and 19). This rectification issue was first examined by *Kessler and Kleeman* [2000] where idealized MJO wind forcing was applied to virtually the same ocean model that is used here. That study found that the low-frequency ocean response to the MJO in the equatorial western Pacific consisted of a cooling (~0.4°C) and eastward current anomaly (~0.2 m s^{-1}). In the present study, the low-frequency ocean response consisted of a much weaker cooling (~0.1°C) in the equatorial western Pacific (and Indian) Ocean region, a relatively larger warming in the maritime continent region (~0.3°C), a fair amount of MLD shallowing (~5 m) in most of the above regions, and a westward equatorial Pacific Ocean current anomaly (~0.1 m s^{-1}). Sensitivity experiments designed to mimic aspects of KK showed that the larger SST cooling in the KK study likely resulted equally from the neglect of the shortwave component of the MJO forcing and the artificial lower limit set for the wind speed (>4 m s^{-1}). The direct effects

associated with the manner that these forcings were handled were compounded by the impacts that they also had on the MLD. For example, in the easterly (i.e., low wind speed) and clear-sky phase of the MJO, both of the above forcing specifications would lead to a much weaker SST warming than if shortwave was included and no wind threshold was utilized. Further, each condition also reduces the amount of MLD shoaling that would typically occur in this phase of the MJO which would tend to limit the SST warming. In addition, the shallowing of the MLD that occurs in the heating/easterly wind phase of the MJO, which was likely to be much more limited in the KK versus the present study, appears to be responsible for the (sign) difference in the low-frequency equatorial western Pacific zonal current anomaly. While the present study utilized what might be considered more realistic MJO forcing conditions given they were constructed from observations and included all components of the forcing, and it employed higher vertical resolution which may play a role in some of the above differences, this should not be taken to mean that the results are more conclusive. Rather, they, along with the KK findings, should be considered with some caution given the rather large sensitivity of the results to the forcing conditions applied. Additional experimentation is needed with other ocean GCMs and alternative forcing scenarios.

[51] In conjunction with the above aspect of the study, it was found that the heat flux variations associated with the MJO produce systematic variations in the east-west zonal gradient of SST (Figure 20). In particular, when the eastern Indian Ocean is undergoing cooling the western Indian Ocean tends to undergo heating, and vice versa. When considered against the background SST gradient, which is weak during boreal winter, these modest variations in basin-wide SST gradient could play a role in the evolution of the IOZM, at least to the extent the Bjerkness mechanism plays a role [e.g., *Saji et al.*, 1999; *Webster et al.*, 1999; *Iizuka et al.*, 2000]. As yet, it is not been conclusively determined the degree this and or other dynamically based mechanisms [e.g., *Hastenrath et al.*, 1993; *Iizuka et al.*, 2000; *Annamalai et al.*, 2003] play a role and/or work together to determine IOZM variability. Further observational study is needed in order to examine the extent to which MJO heat flux forcing might have played a role in the development and/or demise of observed IOZM events. The above MJO-IOZM interactions are noteworthy, since along with the possible influence that the MJO has on the evolution of ENSO [see *Zhang et al.*, 2001], they provide additional examples of roles that the MJO might have in modulating low-frequency aspects of our climate.

[52] **Acknowledgments.** Support for this study was provided by the National Atmospheric and Aeronautics Administration under grants NAG5-11033 (DW, LL) and Salinity, QUICKSCAT, TRMM, and Indian Ocean Biogeochemistry grants (RM) as well as the National Science Foundation under grant ATM-0094416 (DW). We would like to thank William Kessler and James Potemra for their very careful and helpful reviews. In addition, we would like to thank G. Lagerloef for providing the surface current data. This study's analysis and presentation benefited from the use of the NCAR Graphics Package and Seaspace Corporation's TeraScan software system.

References

Anderson, S. P., R. A. Weller, and R. B. Lukas, Surface buoyancy forcing and the mixed layer of the western Pacific warm pool: Observations and 1D model results, *J. Clim.*, *9*, 3056–3085, 1996.

Annamalai, H., R. Murtugudde, J. T. Potemra, S. P. Xie, and B. Wang, Coupled dynamics in the Indian Ocean: Externally triggered or an internal mode?, *Deep Sea Res., Part II*, in press, 2003.

Arakawa, A., and V. R. Lamb, Computational design of the basic dynamical processes of the UCLA general circulation model, in *In Methods in Computational Physics*, edited by J. Chang, pp. 173–265, Academic, San Diego, Calif., 1977.

Atlas, R., R. N. Hoffman, S. C. Bloom, J. C. Jusem, and J. Ardizzone, A multiyear global surface wind velocity dataset using SSM/I wind observations, *Bull. Am. Meteorol. Soc.*, *77*, 869–882, 1996.

Bishop, J. K. B., W. B. Rossow, and E. G. Dutton, Surface solar irradiance from the International Satellite Cloud Climatology Project 1983–1991, *J. Geophys. Res.*, *102*, 6883–6910, 1997.

Bonjean, F., and G. S. E. Lagerloef, Diagnostic model and analysis of the surface currents in the tropical Pacific Ocean, *J. Phys. Oceanogr.*, *32*, 2938–2954, 2002.

Cane, M. A., Response of an equatorial ocean to simple wind stress patterns.1. Model formulation and analytic results, *J. Mar. Res.*, *37*(2), 233–252, 1979.

Chen, D., L. M. Rothstein, and A. J. Busalacchi, A hybrid vertical mixing scheme and its application to tropical ocean models, *J. Phys. Oceanogr.*, *24*, 2156–2179, 1994.

Cronin, M. F., and M. J. McPhaden, The upper ocean heat balance in the western equatorial Pacific warm pool during September–December 1992, *J. Geophys. Res.*, *102*, 8533–8553, 1997.

Delecluse, P., M. K. Davey, Y. Kitamura, S. G. H. Philander, M. Suarez, and L. Bengtsson, Coupled general circulation modeling of the tropical Pacific, *J. Geophys. Res.*, *103*, 14,357–14,373, 1998.

Duchon, C. E., Lanczos filter in one and two dimensions, *J. Appl. Meteorol.*, *18*, 1016–1022, 1979.

Eriksen, C. C., Equatorial ocean response to rapidly translating wind bursts, *J. Phys. Oceanogr.*, *23*, 1208–1230, 1993.

Eriksen, C. C., M. B. Blumenthal, S. P. Hayes, and P. Ripa, Wind-generated equatorial Kelvin waves observed across the Pacific-Ocean, *J. Phys. Oceanogr.*, *13*, 1622–1640, 1983.

Feng, M., R. Lukas, P. Hacker, R. A. Weller, and S. P. Anderson, Upper-ocean heat and salt balances in the western equatorial Pacific in response to the intraseasonal oscillation during TOGA COARE, *J. Clim.*, *13*, 2409–2427, 2000.

Flatau, M., P. J. Flatau, P. Phoebus, and P. P. Niller, The feedback between equatorial convection and local radiative and evaporative processes: The implications for intraseasonal oscillations, *J. Atmos. Sci.*, *54*, 2373–2386, 1997.

Gent, P. R., and M. A. Cane, A reduced gravity, primitive equation model of the upper equatorial ocean, *J. Comput. Phys.*, *81*, 444–480, 1989.

Giese, B. S., and D. E. Harrison, Eastern equatorial Pacific response to 3 composite westerly wind types, *J. Geophys. Res.*, *96*, 3239–3248, 1991.

Gill, A. E., Models of equatorial undercurrents, paper presented at Symposium on Numerical Models of Ocean Circulation, Natl. Acad. of Sci., 1975.

Harrison, D. E., and B. S. Giese, Remote westerly wind forcing of the eastern equatorial Pacific-Some model results, *Geophys. Res. Lett.*, *15*, 804–807, 1988.

Hastenrath, S., A. Nicklis, and L. Greischar, Atmospheric-hydrospheric mechanisms of climate anomalies in the western equatorial Indian Ocean, *J. Geophys. Res.*, *98*, 20,219–20,235, 1993.

Hayashi, Y., and D. G. Golder, United mechanisms for the generation of low- and high-frequency tropical waves. 2. Theoretical interpretations, *J. Meteorol. Soc. Jpn.*, *75*, 775–797, 1997.

Hendon, H. H., Impact of air-sea coupling on the Madden-Julian Oscillation in a general circulation model, *J. Atmos. Sci.*, *57*, 3939–3952, 2000.

Hendon, H. H., and J. Glick, Intraseasonal air-sea interaction in the tropical Indian and Pacific Oceans, *J. Clim.*, *10*, 647–661, 1997.

Hendon, H. H., and B. Liebmann, A composite study of onset of the Australian summer monsoon, *J. Atmos. Sci.*, *47*, 2227–2240, 1990a.

Hendon, H. H., and B. Liebmann, The intraseasonal (30–50 Day) oscillation of the Australian summer monsoon, *J. Atmos. Sci.*, *47*, 2909–2923, 1990b.

Hendon, H. H., and M. L. Salby, The life-cycle of the Madden-Julian Oscillation, *J. Atmos. Sci.*, *51*, 2225–2237, 1994.

Hendon, H. H., B. Liebmann, and J. D. Glick, Oceanic Kelvin waves and the Madden-Julian Oscillation, *J. Atmos. Sci.*, *55*, 88–101, 1998.

Higgins, R. W., and K. C. Mo, Persistent North Pacific circulation anomalies and the tropical intraseasonal oscillation, *J. Clim.*, *10*, 223–244, 1997.

Higgins, R. W., and S. D. Schubert, Simulations of persistent North Pacific circulation anomalies and interhemispheric teleconnections, *J. Atmos. Sci.*, *53*, 188–207, 1996.

Higgins, R. W., and W. Shi, Intercomparison of the principal modes of interannual and intraseasonal variability of the North American Monsoon System, *J. Clim.*, *14*, 403–417, 2001.

Higgins, R. W., J. K. E. Schemm, W. Shi, and A. Leetmaa, Extreme precipitation events in the western United States related to tropical forcing, *J. Clim.*, *13*, 793–820, 2000.

Huang, R. X., Real fresh-water flux as a natural boundary-condition for the salinity balance and thermohaline circulation forced by evaporation and precipitation, *J. Phys. Oceanogr.*, *23*, 2428–2446, 1993.

Iizuka, S., T. Matsuura, and T. Yamagata, The Indian Ocean SST dipole simulated in a coupled general circulation model, *Geophys. Res. Lett.*, *27*, 3369–3372, 2000.

Jones, C., Occurrence of extreme precipitation events in California and relationships with the Madden-Julian Oscillation, *J. Clim.*, *13*, 3576–3587, 2000.

Jones, C., and J. K. E. Schemm, The influence of intraseasonal variations on medium- to extended-range weather forecasts over South America, *Mon. Weather Rev.*, *128*, 486–494, 2000.

Jones, C., D. E. Waliser, and C. Gautier, The influence of the Madden-Julian Oscillation on ocean surface heat fluxes and sea surface temperature, *J. Clim.*, *11*, 1057–1072, 1998.

Kemball-Cook, S., B. Wang, and Z. Fu, Simulation of the ISO in the ECHAM4 model: The impact of coupling with an ocean model, *J. Atmos. Sci.*, *59*, 1433–1453, 2002.

Kessler, W. S., and R. Kleeman, Rectification of the Madden-Julian Oscillation into the ENSO cycle, *J. Clim.*, *13*, 3560–3575, 2000.

Kessler, W. S., M. J. McPhaden, and K. M. Weickmann, Forcing of intraseasonal Kelvin waves in the equatorial Pacific, *J. Geophys. Res.*, *100*, 10,613–10,631, 1995.

Kindle, J. C., and P. A. Phoebus, The ocean response to operational westerly wind bursts during the 1991–1992 El-Nino, *J. Geophys. Res.*, *100*, 4893–4920, 1995.

Kraus, E. B., and J. S. Turner, A one-dimensional model of seasonal thermocline, II, General theory and its consequences, *Tellus*, *19*, 98–105, 1967.

Krishnamurti, T. N., D. K. Oosterhof, and A. V. Mehta, Air sea interaction on the time scale of 30 to 50 days, *J. Atmos. Sci.*, *45*, 1304–1322, 1988.

Lau, K. M., and P. H. Chan, The 40–50 day oscillation and the El-Nino Southern Oscillation—A new perspective, *Bull. Am. Meteorol. Soc.*, *67*, 533–534, 1986a.

Lau, K. M., and P. H. Chan, Aspects of the 40–50 day oscillation during the northern summer as inferred from outgoing longwave radiation, *Mon. Weather Rev.*, *114*, 1354–1367, 1986b.

Lau, K. M., and L. Peng, Origin of low-frequency (intraseasonal) oscillations in the tropical atmosphere. 1. Basic theory, *J. Atmos. Sci.*, *44*, 950–972, 1987.

Lau, K. M., and T. J. Phillips, Coherent fluctuations of extratropical geopotential height and tropical convection in intraseasonal time scales, *J. Atmos. Sci.*, *43*, 1164–1181, 1986.

Lau, K. M., and C. H. Sui, Mechanisms of short-term sea surface temperature regulation: Observations during TOGA COARE, *J. Clim.*, *10*, 465–472, 1997.

Levitus, S., *Climatological Atlas of the World Ocean*, Natl. Oceanic and Atmos. Admin., Silver Spring, Md., 1994.

Li, Z. Q., and H. G. Leighton, Global climatologies of solar-radiation budgets at the surface and in the atmosphere from 5 years of Erbe data, *J. Geophys. Res.*, *98*, 4919–4930, 1993.

Liebmann, B., and D. L. Hartmann, An observational study of tropical midlatitude interaction on intraseasonal time scales during winter, *J. Atmos. Sci.*, *41*, 3333–3350, 1984.

Lorenz, E. N., N-cycle time-differencing scheme for stepwise numerical integration, *Mon. Weather Rev.*, *99*, 644–648, 1971.

Loschnigg, J., and P. J. Webster, A coupled ocean-atmosphere system of SST modulation for the Indian Ocean, *J. Clim.*, *13*, 3342–3360, 2000.

Madden, R. A., and P. R. Julian, Observations of the 40–50-day tropical oscillation—A review, *Mon. Weather Rev.*, *122*, 814–837, 1994.

Maloney, E. D., and D. L. Hartmann, Modulation of eastern North Pacific hurricanes by the Madden-Julian Oscillation, *J. Clim.*, *13*, 1451–1460, 2000a.

Maloney, E. D., and D. L. Hartmann, Modulation of hurricane activity in the Gulf of Mexico by the Madden-Julian Oscillation, *Science*, *287*, 2002–2004, 2000b.

Matsuno, T., Quasi-geostrophic motions in the equatorial area, *J. Meteorol. Soc. Jpn.*, *44*, 25–43, 1966.

McPhaden, M. J., El Nino—The child prodigy of 1997–98, *Nature*, *398*, 559–562, 1999.

McPhaden, M., Mixed layer temperature balance on intraseasonal timescales in the equatorial Pacific Ocean, *J. Clim.*, *15*, 2632–2647, 2002.

McPhaden, M. J., and B. A. Taft, Dynamics of seasonal and intraseasonal variability in the eastern equatorial Pacific, *J. Phys. Oceanogr.*, *18*, 1713–1732, 1988.

McPhaden, M. J., H. P. Freitag, S. P. Hayes, B. A. Taft, Z. Chien, and K. Wyrtki, The response of the equatorial Pacific Ocean to a westerly wind burst in May 1986, *J. Geophys. Res.*, *93*, 10,589–10,603, 1988.

Mo, K. C., Intraseasonal modulation of summer precipitation over North America, *Mon. Weather Rev.*, *128*, 1490–1505, 2000.

Mo, K. C., and R. W. Higgins, The Pacific-South American modes and tropical convection during the Southern Hemisphere winter, *Mon. Weather Rev.*, *126*, 1581–1596, 1998a.

Mo, K. C., and R. W. Higgins, Tropical convection and precipitation regimes in the western United States, *J. Clim.*, *11*, 2404–2423, 1998b.

Mo, K. C., and R. W. Higgins, Tropical influences on California precipitation, *J. Clim.*, *11*, 412–430, 1998c.

Murtugudde, R., and A. J. Busalacchi, Salinity effects in a tropical ocean model, *J. Geophys. Res.*, *103*, 3283–3300, 1998.

Murtugudde, R., and A. J. Busalacchi, Interannual variability of the dynamics and thermodynamics of the tropical Indian Ocean, *J. Clim.*, *12*, 2300–2326, 1999.

Murtugudde, R., R. Seager, and A. Busalacchi, Simulation of the tropical oceans with an ocean GCM coupled to an atmospheric mixed-layer model, *J. Clim.*, *9*, 1795–1815, 1996.

Murtugudde, R., A. J. Busalacchi, and J. Beauchamp, Seasonal-to-interannual effects of the Indonesian Throughflow on the tropical Indo-Pacific Basin, *J. Geophys. Res.*, *103*, 21,425–21,441, 1998.

Murtugudde, R., J. Beauchamp, C. McClain, M. Lewis, and A. Busalacchi, Effects of penetrative radiation on the upper tropical ocean circulation, *J. Clim.*, *15*, 470–486, 2002.

Myers, D., and D. E. Waliser, Three dimensional water vapor and cloud variations associated with the Madden-Julian Oscillation during Norhtern Hemisphere winter, *J. Clim.*, in press, 2003.

NoguesPaegle, J., and K. C. Mo, Alternating wet and dry conditions over South America during summer, *Mon. Weather Rev.*, *125*, 279–291, 1997.

Paegle, J. N., L. A. Byerle, and K. C. Mo, Intraseasonal modulation of South American summer precipitation, *Mon. Weather Rev.*, *128*, 837–850, 2000.

Potemra, J. T., S. L. Hautala, J. Sprintall, and W. Pandoe, Interaction between the Indonesian Seas and the Indian Ocean in observations and numerical models, *J. Phys. Oceanogr.*, *32*, 1838–1854, 2002.

Price, J. F., R. A. Weller, and R. Pinkel, Diurnal cycling—Observations and models of the upper ocean response to diurnal heating, cooling, and wind mixing, *J. Geophys. Res.*, *91*, 8411–8427, 1986.

Ralph, E. A., K. N. Bi, P. P. Niiler, and Y. duPenhoat, A Lagrangian description of the western equatorial Pacific response to the wind burst of December 1992: Heat advection in the warm pool, *J. Clim.*, *10*, 1706–1721, 1997.

Reynolds, R. W., and T. M. Smith, Improved global sea-surface temperature analyses using optimum interpolation, *J. Clim.*, *7*, 929–948, 1994.

Robinson, A. R., An investigation into the wind as the cause of the equatorial undercurrent, *J. Mar. Res.*, *24*, 179–204, 1966.

Rossow, W. B., and R. A. Schiffer, ISCCP cloud data products, *Bull. Am. Meteorol. Soc.*, *72*, 2–20, 1991.

Saji, N. H., B. N. Goswami, P. N. Vinayachandran, and T. Yamagata, A dipole mode in the tropical Indian Ocean, *Nature*, *401*, 360–363, 1999.

Seager, R., and M. B. Blumenthal, modeling tropical Pacific sea-surface temperature with satellite-derived solar radiative forcing, *J. Clim.*, *7*, 1943–1957, 1994.

Seager, R., M. B. Blumenthal, and Y. Kushnir, An advective atmospheric mixed-layer model for ocean modeling purposes—Global simulation of surface heat fluxes, *J. Clim.*, *8*, 1951–1964, 1995.

Shapiro, R., Smoothing, filtering and boundary effects, *Rev. Geophys.*, *8*, 359–387, 1970.

Shinoda, T., and H. H. Hendon, Mixed layer modeling of intraseasonal variability in the tropical western Pacific and Indian Oceans, *J. Clim.*, *11*, 2668–2685, 1998.

Shinoda, T., and H. H. Hendon, Upper-ocean heat budget in response to the Madden-Julian Oscillation in the western equatorial Pacific, *J. Clim.*, *14*, 4147–4165, 2001.

Shinoda, T., H. H. Hendon, and J. Glick, Intraseasonal variability of surface fluxes and sea surface temperature in the tropical western Pacific and Indian Oceans, *J. Clim.*, *11*, 1685–1702, 1998.

Shinoda, T., H. H. Hendon, and J. Glick, Intraseasonal surface fluxes in the tropical western Pacific and Indian Oceans from NCEP reanalyses, *Mon. Weather Rev.*, *127*, 678–693, 1999.

Slingo, J. M., et al., Intraseasonal oscillations in 15 atmospheric general circulation models: Results from an AMIP diagnostic subproject, *Clim. Dyn.*, *12*, 325–357, 1996.

Slingo, J. M., D. P. Rowell, K. R. Sperber, and E. Nortley, On the predictability of the interannual behaviour of the Madden-Julian Oscillation and its relationship with El Nino, *Q. J. R. Meteorol. Soc.*, *125*, 583–609, 1999.

Sprintall, J., A. L. Gordon, R. Murtugudde, and R. D. Susanto, A semiannual Indian Ocean forced Kelvin wave observed in the Indonesian seas in May 1997, *J. Geophys. Res*, *105*(C7), 17,217–17,230, 2000.

Stockdale, T. N., A. J. Busalacchi, D. E. Harrison, and R. Seager, Ocean modeling for ENSO, *J. Geophys. Res.*, *103*, 14,325–14,355, 1998.

Vecchi, G. A., and D. E. Harrison, Tropical Pacific sea surface temperature anomalies, El Nino, and equatorial westerly wind events, *J. Clim.*, *13*, 1814–1830, 2000.

Waliser, D. E., Formation and limiting mechanisms for very high sea surface temperature: Linking the dynamics and the thermodynamics, *J. Clim.*, *9*, 161–188, 1996.

Waliser, D. E., B. Blanke, J. D. Neelin, and C. Gautier, Shortwave feedbacks and El Nino–Southern Oscillation: Forced ocean and coupled ocean-atmosphere experiments, *J. Geophys. Res.*, *99*, 25,109–25,125, 1994.

Waliser, D. E., K. M. Lau, and J. H. Kim, The influence of coupled sea surface temperatures on the Madden-Julian Oscillation: A model perturbation experiment, *J. Atmos. Sci.*, *56*, 333–358, 1999.

Waliser, D. E., et al., AGCM simulations of intraseasonal variability associated with the Asian summer monsoon, *Clim. Dyn.*, in press, 2003.

Wang, B., and H. Rui, Synoptic climatology of transient tropical intraseasonal convection anomalies—1975–1985, *Meteorol. Atmos. Phys.*, *44*, 43–61, 1990.

Wang, B., and X. S. Xie, A model for the boreal summer intraseasonal oscillation, *J. Atmos. Sci.*, *54*, 72–86, 1997.

Wang, B., and X. S. Xie, Coupled modes of the warm pool climate system. part 1: The role of air-sea interaction in maintaining Madden-Julian Oscillation, *J. Clim.*, *11*, 2116–2135, 1998.

Webster, P. J., A. M. Moore, J. P. Loschnigg, and R. R. Leben, Coupled ocean-atmosphere dynamics in the Indian Ocean during 1997–98, *Nature*, *401*, 356–360, 1999.

Weickmann, K. M., Intraseasonal circulation and outgoing longwave radiation modes during Northern Hemisphere winter, *Mon. Weather Rev.*, *111*, 1838–1858, 1983.

Weickmann, K. M., El Nino-Southern Oscillation and Madden-Julian (30–60 day) Oscillations during 1981–1982, *J. Geophys. Res.*, *96*, 3187–3195, 1991.

Weickmann, K. M., G. R. Lussky, and J. E. Kutzbach, Intraseasonal (30–60 day) fluctuations of outgoing longwave radiation and 250-Mb streamfunction during northern winter, *Mon. Weather Rev.*, *113*, 941–961, 1985.

Weller, R. A., and S. P. Anderson, Surface meteorology and air-sea fluxes in the western equatorial Pacific warm pool during the TOGA coupled ocean-atmosphere response experiment, *J. Clim.*, *9*, 1959–1990, 1996.

Woolnough, S. J., J. M. Slingo, and B. J. Hoskins, The relationship between convection and sea surface temperature on intraseasonal timescales, *J. Clim.*, *13*, 2086–2104, 2000.

Xie, P. P., and P. A. Arkin, Global precipitation: A 17-year monthly analysis based on gauge observations, satellite estimates, and numerical model outputs, *Bull. Am. Meteorol. Soc.*, *78*, 2539–2558, 1997.

Yasunari, T., A quasi-stationary appearance of the 30–40 day period in the cloudiness fluctuations during the summer monsoon over India, *J. Meteorol. Soc. Jpn.*, *59*, 336–354, 1980.

Zhang, C. D., Atmospheric intraseasonal variability at the surface in the tropical western Pacific Ocean, *J. Atmos. Sci.*, *53*, 739–758, 1996.

Zhang, C. D., Intraseasonal perturbations in sea surface temperatures of the equatorial eastern Pacific and their association with the Madden-Julian Oscillation, *J. Clim.*, *14*, 1309–1322, 2001.

Zhang, C. D., and M. J. McPhaden, Intraseasonal surface cooling in the equatorial western Pacific, *J. Clim.*, *13*, 2261–2276, 2000.

Zhang, C., H. H. Hendon, W. S. Kessler, and A. Rosati, A workshop on the MJO and ENSO, *Bull. Am. Meterol. Soc.*, *82*, 971–976, 2001.

Zhang, K. Q., and L. M. Rothstein, Modeling the oceanic response to westerly wind bursts in the western equatorial Pacific, *J. Phys. Oceanogr.*, *28*, 2227–2249, 1998.

Zveryaev, I., II, Interdecadal changes in the zonal wind and the intensity of intraseasonal oscillations during boreal summer Asian monsoon, *Tellus, Ser. A*, *54*, 288–298, 2002.

L. E. Lucas and D. E. Waliser, Marine Sciences Research Center, Endeavour Hall 205, State University of New York, Stony Brook, NY 11794-5000, USA. (duane.waliser@sunysb.edu)

R. Murtugudde, Earth System Science Interdisciplinary Center, University of Maryland, College Park, MD 20742, USA.